Report to Sandia Laboratory on University of Wisconsin Fusion Engineering Program Design Activities for the Light Ion Beam Fusion Target Development Facility from August 1980 to August 1981

B. Badger, R.L. Engelstad, G.L. Kulcinski, E.G. Lovell, T.J. McCarville, G.A. Moses, R.R. Peterson, I.N. Sviatoslavsky, and M.A. Sweeney

September 1981

UWFDM-414

FUSION TECHNOLOGY INSTITUTE

UNIVERSITY OF WISCONSIN

MADISON WISCONSIN

Report to Sandia Laboratory on University of Wisconsin Fusion Engineering Program Design Activities for the Light Ion Beam Fusion Target Development Facility from August 1980 to August 1981

B. Badger, R.L. Engelstad, G.L. Kulcinski, E.G. Lovell, T.J. McCarville, G.A. Moses, R.R. Peterson, I.N. Sviatoslavsky, and M.A. Sweeney

Fusion Technology Institute
University of Wisconsin
1500 Engineering Drive
Madison, WI 53706

http://fti.neep.wisc.edu

September 1981

UWFDM-414

Report to Sandia Laboratory on University of Wisconsin Fusion Engineering Program Design Activities for the Light Ion Beam Fusion Target Development Facility from August 1980 to August 1981

B. Badger, R.L. Engelstad, G.L. Kulcinski, E.G. Lovell, T.J. McCarville, G.A. Moses, R.R. Peterson, I.N. Sviatoslavsky, and M.A. Sweeney*

Fusion Engineering Program
Nuclear Engineering Department
University of Wisconsin-Madison
Madison, Wisconsin 53706

September 1981

UWFDM-414

*At Sandia Laboratory.

Introduction

This document is a report submitted to Sandia National Laboratory to fulfill the reporting requirements for work completed between the approximate dates of August 1980 to August 1981. It is written in chapter form because it was intended that it would be inserted into a larger Sandia report covering the entire TDF design.

VII. Cavity Gas Response to Target Explosion

VII.A. Introduction

First wall survivability is a critical problem to all ICF reactor designs.[1-6] These problems are also important to the Target Development Facility. The largest potential for damage to the first wall of a light ion beam fusion cavity is not directly from the target explosion generated ions and x-rays because they will be stopped in the 10-100 torr of cavity gas provided $Z > 10$. It should be noted that only "soft" x-rays, below about 1 keV, are necessarily stopped this effectively.[7] Higher energy x-rays will tend to penetrate deeper into the gas, possibly reaching the reactor first wall. However, these "hard" x-rays should not greatly damage wall components because of their long stopping lengths in the wall material. The deposition of this energy into the gas creates a fireball which may propagate to the wall with its possibly damaging overpressure and flux of radiant heat.[8-12] Since the characteristics of the fireball are to a large degree determined by the propagation of radiation through the gas, the heat fluxes and overpressures at the first wall of the reactor may be controlled by the optical properties of the cavity gas. In this section we show that a cavity gas of argon that would have a pressure of 50 torr at 0°C mixed with 0-2% by volume with sodium vapor can provide adequate protection for a reactor first wall. The argon can easily stop the target generated soft x-rays and ion debris while the sodium controls the opacity of the gas. In this section, we describe the numerical techniques used in modeling these phenomena and compare the results predicted by two different computer techniques: single frequency group and multi-frequency groups.

VII.B. Gaseous Mixtures of Sodium and Argon

We have studied the ionization and internal energy of mixtures of monatomic gases and the interaction of radiation with such mixtures.[13,14] The radiation stopping processes considered are photo-ionization, inverse Bremsstrahlung, Thomson scattering and atomic line absorption. These processes are assumed to act independently for each gas in the mixture. Atomic transitions associated with radiation absorptions are assumed to obey a semi-classical formalism.[11] In this approximation, the scattering cross sections for photo-ionization, inverse Bremsstrahlung, Thomson scattering and atomic line absorption are, respectively,[13]

$$\sigma_{ph,i}(\nu,n) = \frac{64\ \pi^4}{3\sqrt{3}} \frac{e^{10} m_e (m_i)^4}{h^6 c \nu^3 n^5} \quad , \qquad \text{(VII-1)}$$

$$\sigma_{Brem,\nu,i}(m_i) = 2.4 \times 10^{-37}\ N_e m_i^2/(h\nu)^3\ \sqrt{T_p}\ cm^2 \quad , \qquad \text{(VII-2)}$$

$$\sigma_{sc,i} = Z_i \left(\frac{e^2}{m_e c^2}\right)^2 \frac{8\pi}{3} \quad , \qquad \text{(VII-3)}$$

and

$$\sigma_{line,i}(n,n',\nu) = 2.78 \times 10^{-18}\ H(\nu,\nu_0,\Delta E) f_{n,n'}\ cm^2 \quad . \qquad \text{(VII-4)}$$

Here, e is the electronic charge, m_e is the electron mass, m_i is the ionization state of the gas atom of species i, $h\nu$ is the energy of a photon in eV and n is the principal quantum number. T_p is the temperature of the mixture of gases in eV, N_e is the electron density, c is the speed of light and Z_i is the atomic number of the gas of species i. ν_0 is the natural frequency of the atomic line, ΔE is its width, H is the shape of the line and $f_{n,n'}$ is its

oscillator strength. The total absorption coefficient for the gas becomes

$$\kappa_\nu = \sum_i \sum_m \sum_{n=1}^{\infty} N_{n,i}(m)\left(\sigma_{ph,i}(\nu,n) + \sigma_{Brem,\nu,i}(m) + \sigma_{sc,i} + \sum_{n'=n+1}^{\infty} \sigma_{line,i}(n,n',\nu)\right) , \tag{VII-5}$$

where $N_{n,i}(m)$ is the density of atoms of species i in the m^{th} ionization state and with principal quantum number n.

We have considered gas mixtures that are assumed to be dense enough to obey the simple form of the Saha equation,[11]

$$I_i(\bar{m}_i + \tfrac{1}{2}) = T_p \ln\left(\frac{AT_p^{3/2}}{N_e}\right) . \tag{VII-6}$$

Here, I_i is the piecewise linear continuous form of the ionization potential of the i^{th} gas species, and $\bar{m}_i$ is the average ionization state of that species. $A = 6.04 \times 10^{21}$ $eV^{-3/2}$. Since N_e is the sum of the electrons ionized from all of the gas species per unit volume, that is,

$$N_e = \sum_{i=1} \bar{m}_i N_i , \tag{VII-7}$$

where N_i is the density of atoms of species i, we must solve a set of Saha equations coupled through N_e. Physically, the Saha model assumes that ionization is balanced with three-body recombination so that when electrons are added from additional ion species, $\bar{m}_i$ for the original species decreases. This effect is most important for species that contribute just a small percent to the total number of atoms, because the electron density is much different

from the density that would be present if the other species were absent. On the other hand, gases that make up a large fraction of the mixture will experience close to the same number of collisions with electrons as they would if there were no other gases present, so their ionization states will not change much.

One important effect of this change in ionization states is the manner in which the radiation mean free paths must be calculated. Two important spectrum averaged radiation mean free paths are the Planck,

$$\ell_1 = \frac{U}{\int_0^\infty \kappa_\nu U_\nu \, d\nu} \qquad \text{(VII-8)}$$

and the Rosseland,

$$\ell \equiv \frac{\int_0^\infty \frac{1}{\kappa_\nu} (dU_\nu/dT_R) \, d\nu}{dU/dT_R} \qquad \text{(VII-9)}$$

where U is the integrated radiant energy density, U_ν is the Planck spectrum, and T_R is the blackbody radiation temperature. If the ionization states of each of the species were independent, so would be the absorption coefficients for each species, neglecting such effects as additional pressure line broadening. The Planck mean free path could then be found from

$$\frac{1}{\ell_1'} = \sum_i \frac{1}{\ell_{1,i}} \quad , \qquad \text{(VII-10)}$$

where $\ell_{1,i}$ is the Planck mean free path for radiation passing through gas type i alone and ℓ_1' is the independently calculated Planck mean free path. The question of interdependence has been tested for a mixture of 1.8×10^{18} cm^{-3}

argon and 3.6×10^{16} cm^{-3} sodium. The results of this test are shown for various equilibrium ($T_R = T_P$) temperatures in Table VII-1. It may be noted that the interdependence is most important at lower temperatures. Because the discrepancy between ℓ_1 and ℓ_1' is so great at lower temperatures, it is important to solve a set of coupled Saha equations when one is dealing with monatomic gases seeded with small amounts of other gases.

In addition to the total mean free paths, the energy density and ionization must be found for the mixture as a whole. The energy density is the total internal energy divided by the total mass; that is,

$$\varepsilon = \left[\sum_i N_i \left\{I_i(\bar{m}_i) + \sum_{j=1}^{j_m} I_i(j) + (1 + \bar{m}_i)T_P\right\}\right] / \left(\sum_i N_i M_i\right) \quad . \qquad \text{(VII-11)}$$

Here, j_m is the largest integer $< \bar{m}_i$ and M_i is the mass of an atom of species i. The ionization state is just the total number of electrons divided by the total number of ions,

$$\bar{m} = \sum_i N_i \bar{m}_i / \sum_i N_i \quad . \qquad \text{(VII-12)}$$

In Fig. VII-1, we show the Planck mean free path for 1.8×10^{18} cm^{-3} argon for concentrations of sodium ranging from 0% to 2% by volume. The densities are expressed in terms of the partial pressure in torr the gas would have at room temperature. From this graph, where the gas temperature equals the radiation temperature, it is clear that low temperature radiation passes through the gas very easily compared to high temperature radiation. This occurs because photo-ionization, the strongest mechanism of photo-absorption, cannot occur with photons less energetic than the ionization potential of the

TABLE VII-1

INTERDEPENDENT AND INDEPENDENT PLANCK MEAN FREE PATHS

$N_{argon} = 1.8 \times 10^{18}\ cm^{-3}$

$N_{sodium} = 3.6 \times 10^{16}\ cm^{-3}$

T (eV)	ℓ_1 (cm)	$\ell_1$argon (cm)	$\ell_1$sodium (cm)	ℓ_1'* (cm)
0.4	128	6.87×10^4	16.0	16.0
0.58	34	2.38×10^4	4.79	4.79
0.85	50.2	243	11.7	11.2
1.23	44.9	10.5	64.9	9.0

* $\frac{1}{\ell_1'} \equiv \frac{1}{\ell_1 \text{sodium}} + \frac{1}{\ell_1 \text{argon}}$

Fig. VII-1

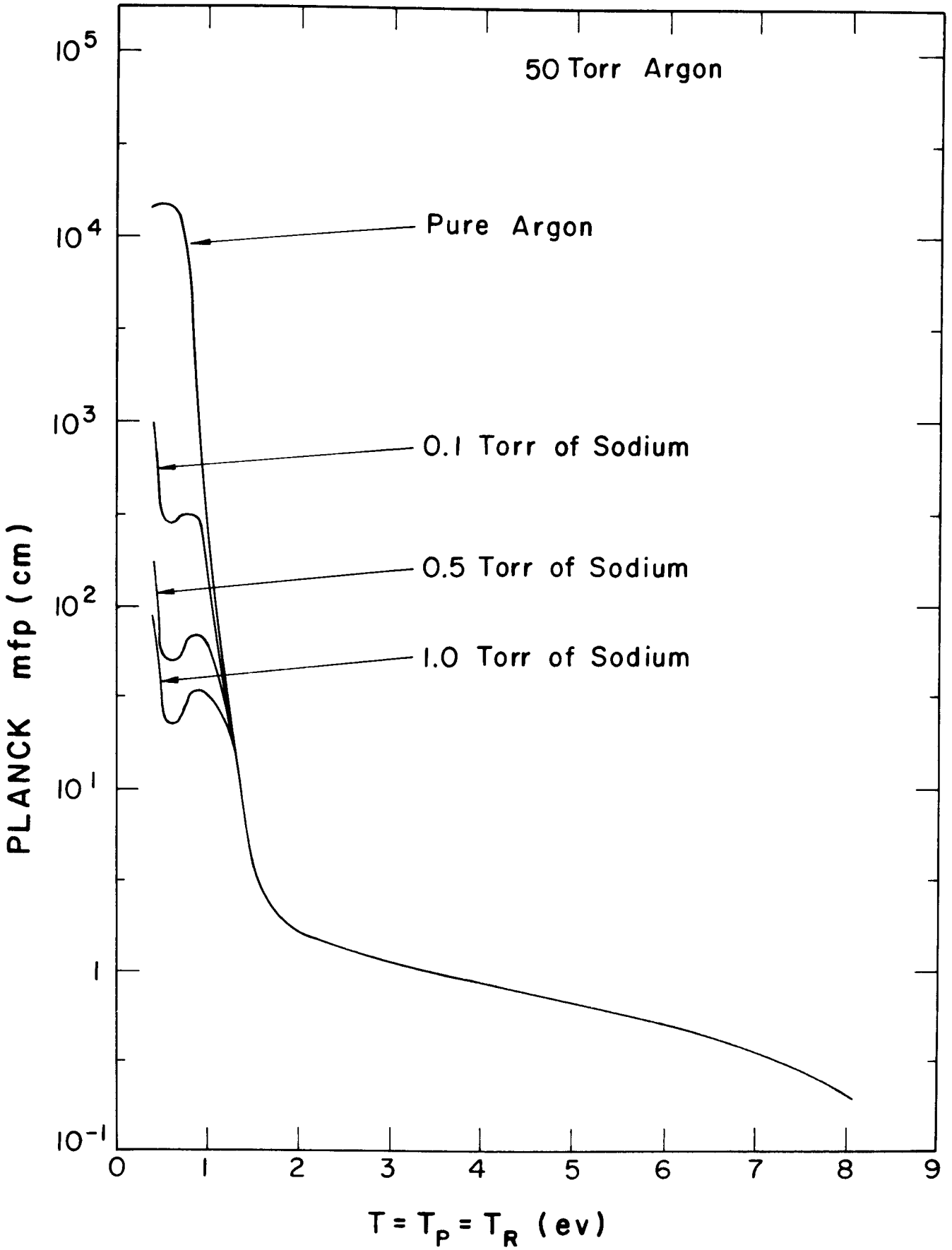

Fig. VII-1. Planck mean free path vs. temperature for various concentrations of sodium mixed with 1.8×10^{18} cm^{-3} argon. Here the radiation is in equilibrium with the gas at temperature T.

gas. Since the ionization potential of argon is higher than that of sodium, higher energy photons will pass through argon than through sodium so that the addition of sodium to argon should decrease the low temperature mean free paths. This effect is clearly shown in Fig. VII-1.

VII.C. Single Frequency Group Fireball Calculations

Once the optical properties of the gas are known, the physics of the fireball propagation may be studied.[15-22] As stated earlier, the argon will absorb most of the target generated x-rays and the ion debris in a small volume, creating a hot fireball at the center of the cavity which is surrounded by cold gas. Initially, the radiation mean free paths are long in the fireball but short in the cold gas so that a wave of heat moves into the cold gas by successive warming of layers of gas near the fireball. Initially this heating wave, whose speed decreases with decreasing fireball temperature, propagates more rapidly than the sound speed. As the fireball expands and cools, the speed of the heating wave drops to the speed of sound and a shock wave is formed which breaks away from the fireball. The fireball continues expanding and cooling until the mean free paths for fireball radiation in the cold gas are longer than the distance to the first wall, at which time the fireball begins radiating its energy to the wall. This continues until the fireball cools to the point where radiation is no longer emitted by the gas and the flow of radiant energy ceases. The effect of decreasing the mean free paths to low energy photons in the cold gas is to slow the propagation of the radiation to the wall. Thus, by adjusting the opacity through variations in the sodium concentration, one may control the total amount of heat radiated to the wall per explosion and the rate at which this heat reaches the wall.

At the University of Wisconsin, a hydrodynamic radiative transfer computer code, FIRE, has been used to simulate this behavior in fireballs.[15-19] FIRE is a one-dimensional hydrodynamics code that calculates the dynamics of two fluids; the plasma at its own temperature and radiation at its own temperature. The transport of the radiation fluid is flux limited and upstream averaged.

A series of fireball calculations have been performed with FIRE for a pellet explosion in a light ion beam reactor cavity. The parameters used and the results are outlined in Table VII-2. The calculations have been done with sodium concentrations ranging from 0% to 2%. The most important results for first wall survivability are the radiant heat flux and the overpressure. These are shown for the largest (2%) and the smallest (0%) sodium concentrations in Figs. VII-2 and VII-3, respectively. These results indicate that the heat flux for 2% sodium is held very effectively behind the shock front, and that the first wall has an insignificant temperature rise. On the other hand, when the cavity gas is pure argon, the heat flux reaches the first wall long before the shock wave does, and the heat flux reaches a much higher maximum. From these two calculations, the effect of the sodium is evident, and this becomes even more clear in Fig. VII-4, which is a plot of the total energy radiated (E_{out}), the maximum overpressure (ΔP), and the maximum heat flux (q_{max}) versus the sodium concentration. When the sodium concentration is less than 0.2%, the wall response is most sensitive to sodium concentration so we tried this as an operating point. The heat flux and overpressure for 0.2% sodium are shown in Fig. VII-5. This case has important advantages over the two previous cases because the maximum heat flux is low enough that the maximum wall temperature difference is tolerable (59.1 K for a 5.0 cm thick

TABLE VII-2

PARAMETERS AND RESULTS OF FIREBALL CALCULATIONS

Wall Radius = 3 meters

Initial Gas Temperature = 0.1 eV

Argon Density = 1.8×10^{18} cm^{-3}

Initial Energy of Fireball = 30 MJ

	Sodium Concentration (%)				
	0.0	0.1	0.2	1.0	2.0
Energy Radiated* (MJ)	2.04	1.44	1.40	1.17	0.93
Shock Pressure (MPa)	.621	.640	.697	.873	.965
Max. Heat Flux to Wall (kW/cm^2)	2.47	1.65	1.15	1.77	1.59

* Energy radiated to first wall in the first 1.5 msec following the target explosion

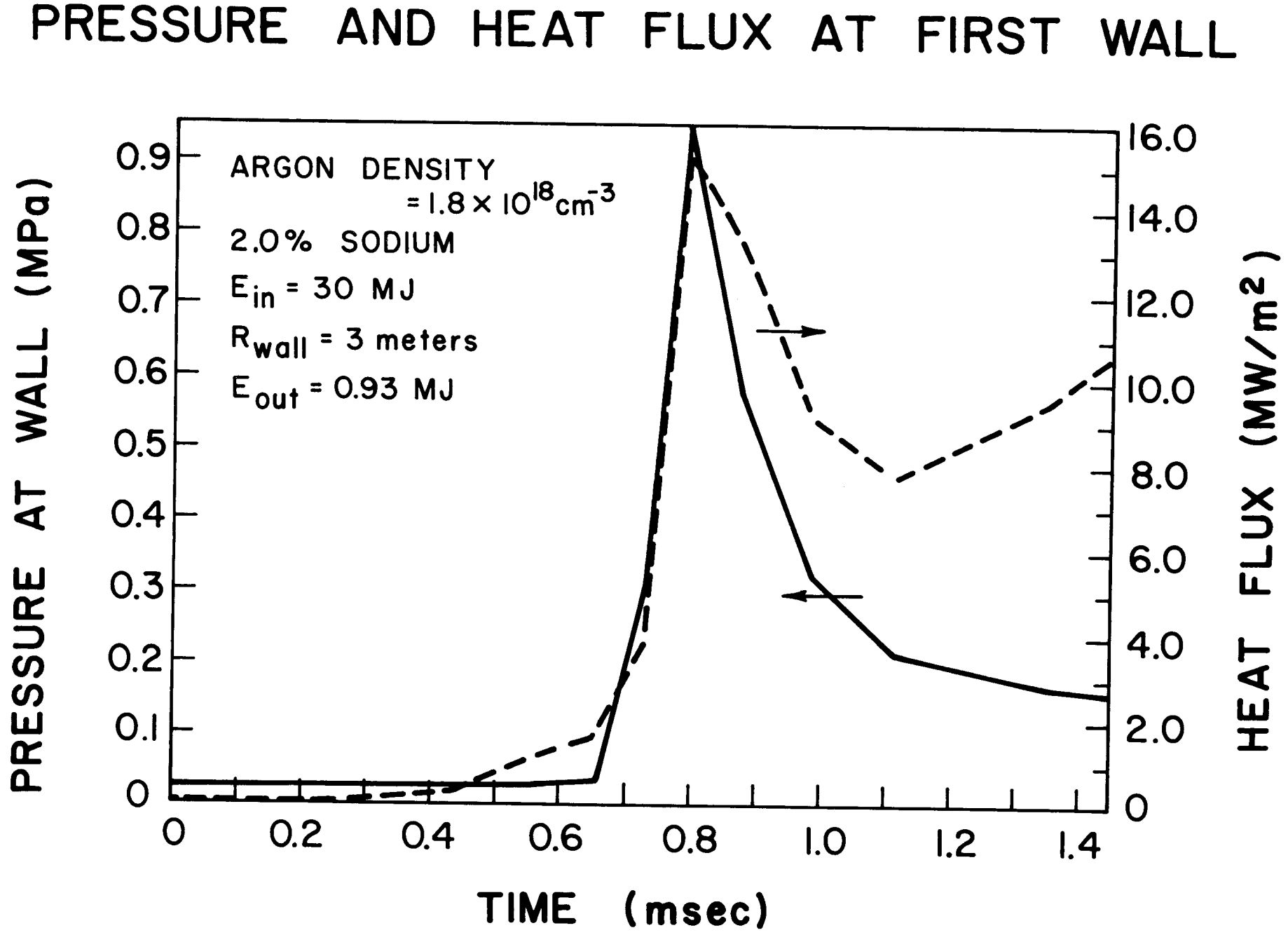

Fig. VII-2. Pressure and heat flux at a three-meter first wall vs. time. A 30 MJ explosion sends a blast wave through 1.8×10^{18} cm^{-3} of 0.1 eV argon gas which is mixed with 2% by volume of sodium.

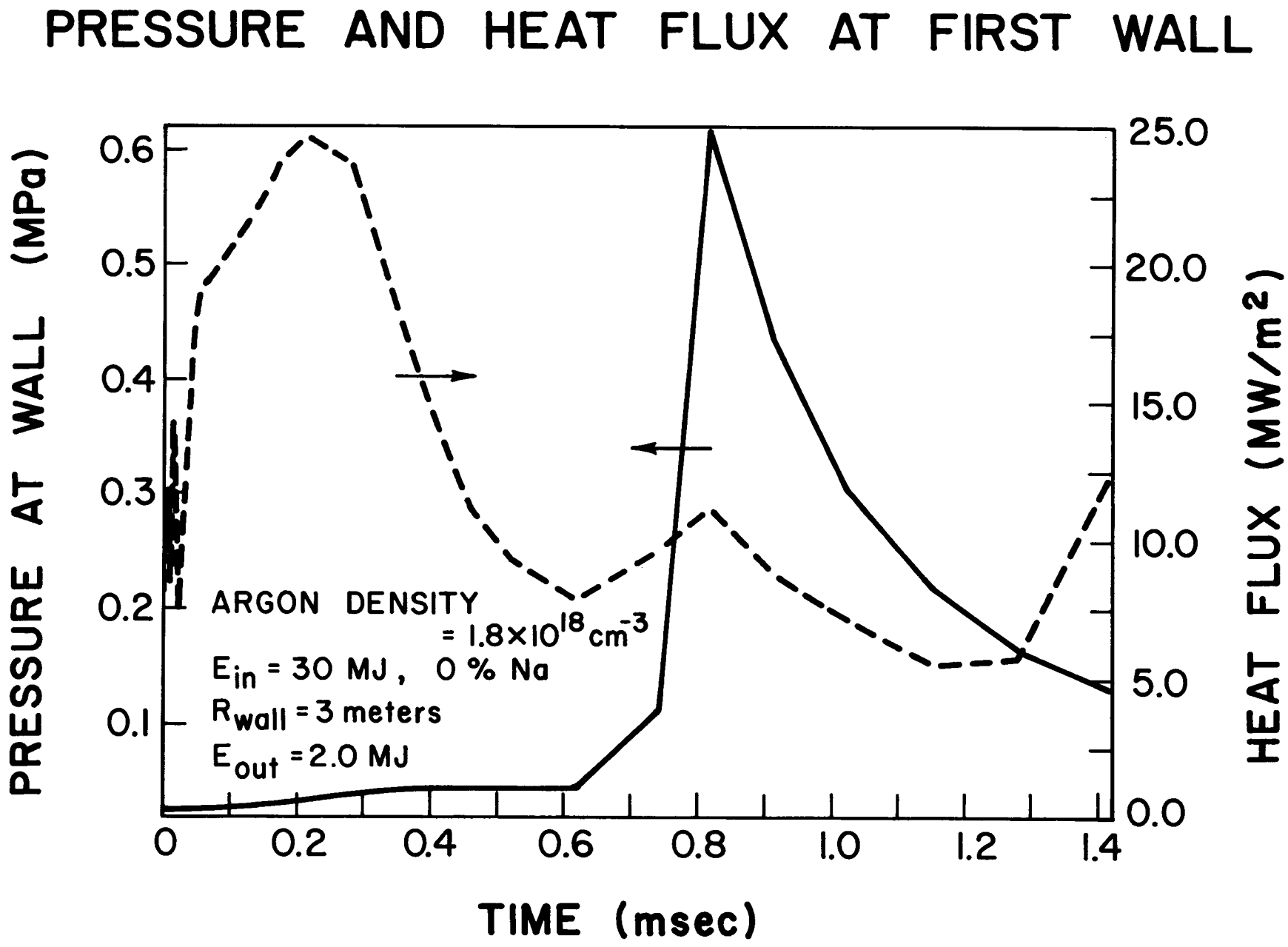

Fig. VII-3. Pressure and heat flux at a three-meter first wall vs. time. This case is the same as Fig. VII-2, except that the gas is pure argon.

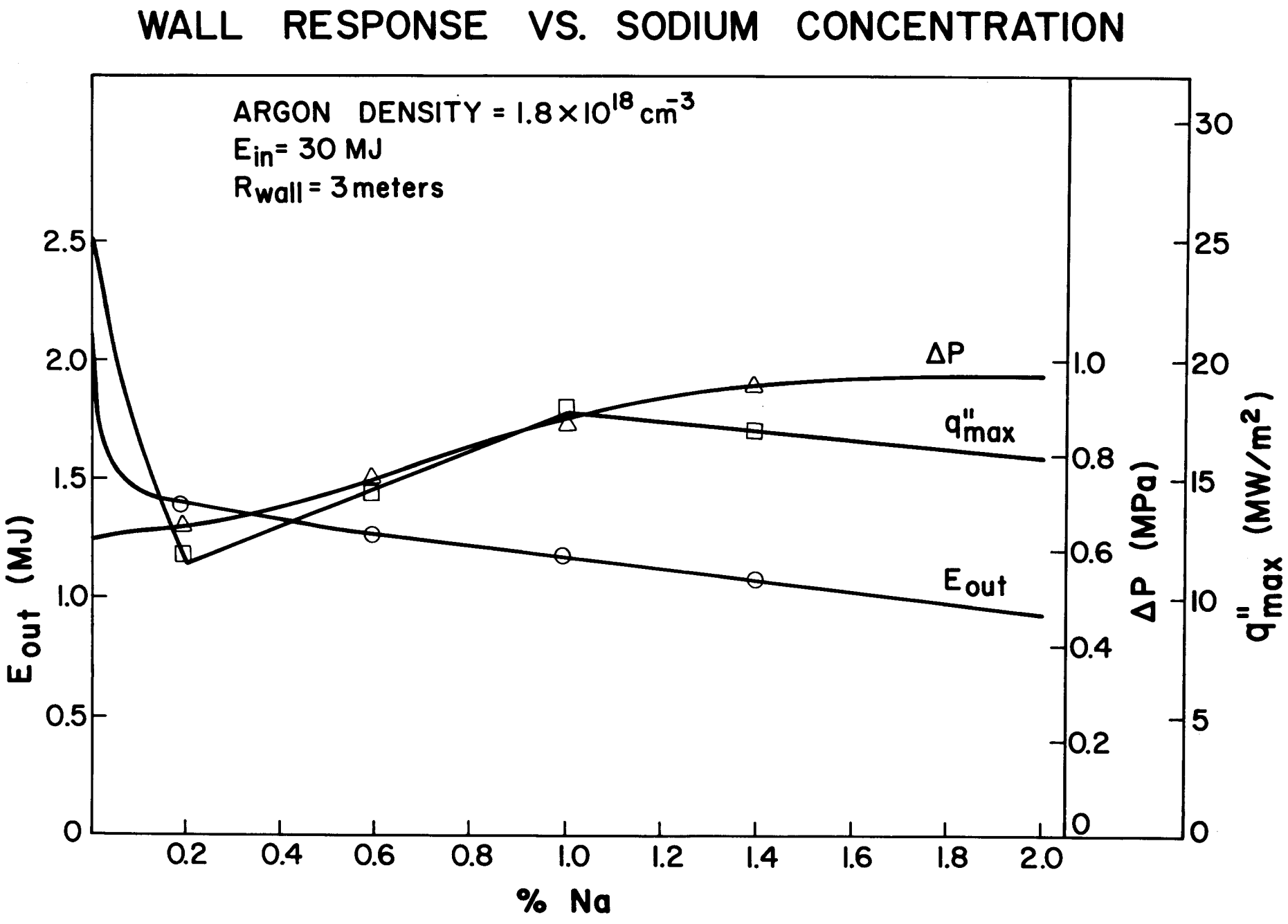

Fig. VII-4. Maximum overpressure, maximum heat flux and energy radiated in the first 2.5 msec at a three-meter radius first wall vs. sodium concentration. Everything but the sodium concentration is the same as in Fig. VII-2.

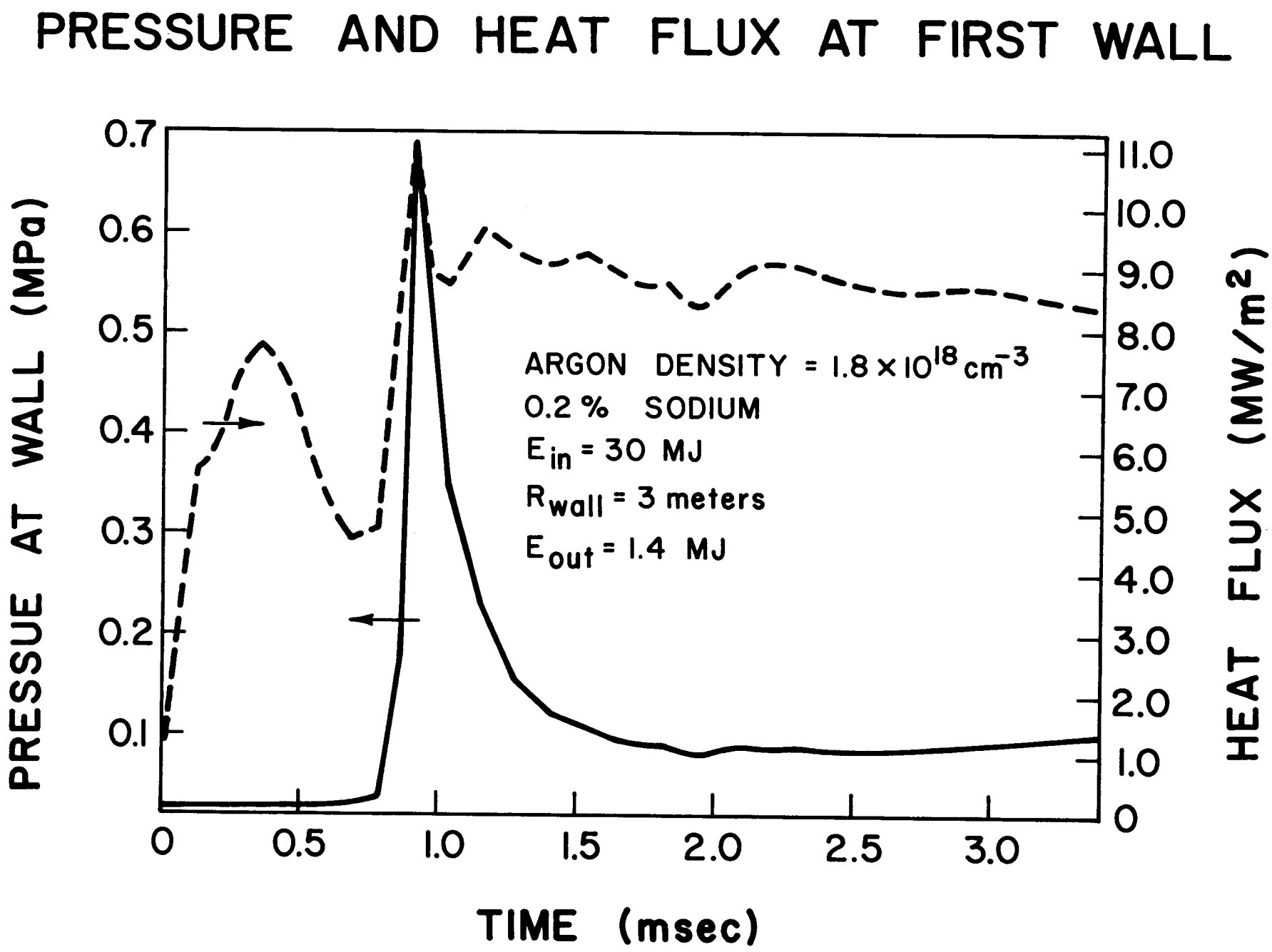

Fig. VII-5. Pressure and heat flux at a three-meter radius first wall. This case is the same as Fig. VII-2, except that the sodium concentration is 0.2%.

stainless steel wall), while the heat reaches the wall in a very broad pulse so that significant energy can be extracted from the gas. For all three cases, a reactor wall can be constructed to survive the structural problems associated with the overpressures.[23]

VII.D. Multifrequency Fireball Calculations

Additional multigroup radiation, two temperature ($T_e = T_i$, $T_r \neq T_e$) thermal transport/hydrodynamic calculations[20] have been done for the gas-filled reactor cavity approach to particle-beam fusion, using the 1-D Lagrangian code CHARTB.[24] This code assumes a Rosseland mean opacity for each energy group of photons with the Planck mean opacity equal to the Rosseland mean if sufficient numbers of groups are used. The multifrequency opacity data were supplied by LANL.[25] A multigroup treatment allows us to obtain the x-ray spectrum as well as the total heat flux at the first wall and provides a more accurate opacity representation, since the opacity can vary by many orders of magnitude as the photon energy changes, as shown in Fig. VII-6.

Initial scoping studies[21,26] at Sandia National Laboratories, assuming no hydrodynamic effects (i.e. without convection) and a single radiation group, showed that the transport of the non-neutronic energy to the wall is slow. Qualitatively, the more accurate single-group calculations at the University of Wisconsin and the Sandia multigroup calculations confirm this previous result. We find that both air and argon act somewhat like large thermal capacitors, absorbing non-neutronic pellet energy rapidly and releasing it over many milliseconds. For example, the 10 ns x-ray pulse in the absence of gas protection is converted into a pulse of approximately 0.1 ms duration at the first wall.[22]

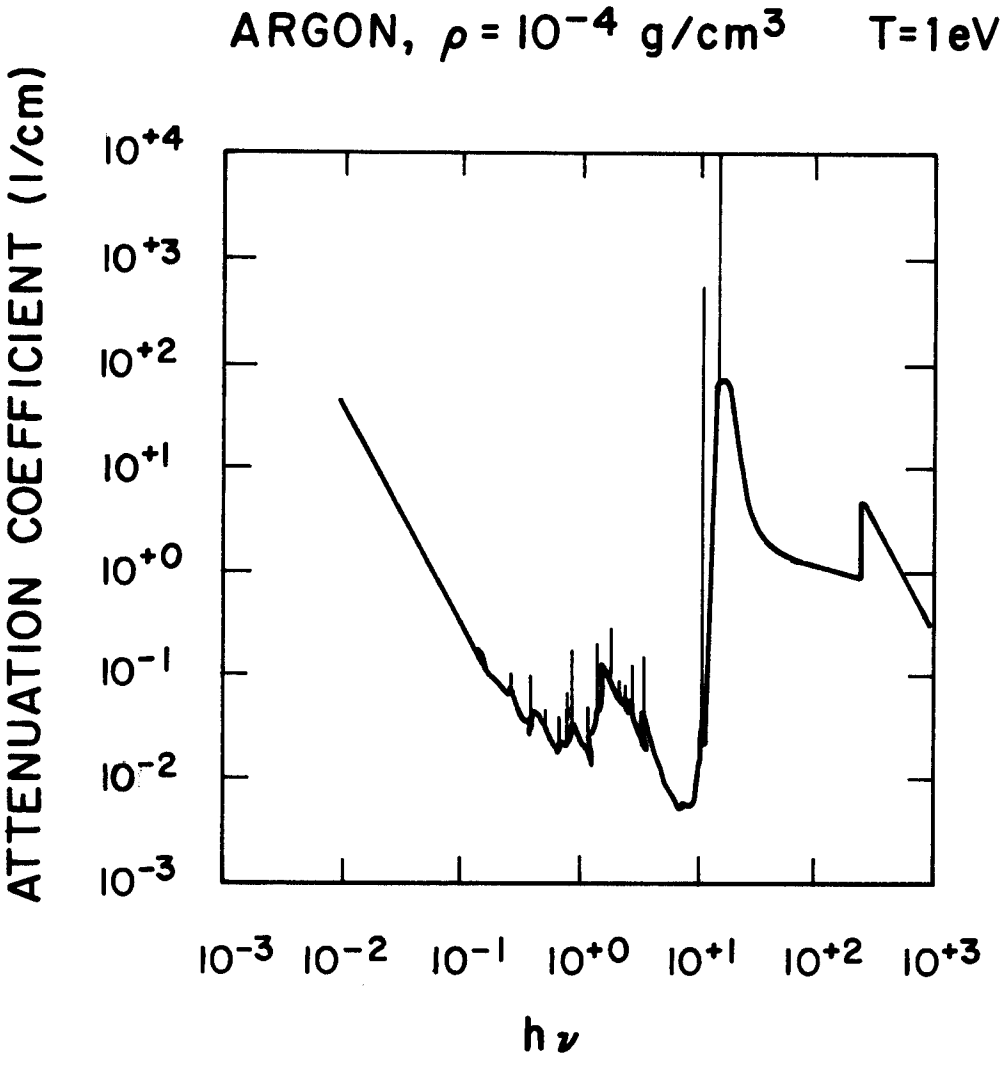

Fig. VII-6. Attenuation coefficient for argon as a function of photon energy (in eV) at a material temperature of 1 eV and a density of 1 x 10^{-4} g/cm^3. Values for photon energies below 13 eV were obtained from Group T4 at Los Alamos National Laboratory (cf. ref. 25). Above 13 eV, analytic fits to the Nuclear Data Tables are used [E. Storm and H.I. Isreal, Nuclear Data Tables A7, 565-581 (1970)].

Deposition of non-neutronic energy from the pellet implosion produces a hot, optically thick "fireball" of small radius in the gas-filled chamber. Multigroup simulations were performed using the following initial conditions: 50 torr of a gas at 750 K with 23.5 MJ of energy absorbed in a 40 cm radius. For argon, such an absorption length corresponds to a blackbody spectrum of approximately 1 keV from a 75 MJ yield pellet, omitting only the high energy tail of the spectrum; the ion debris is stopped in $\lesssim$ 1 cm.

If argon is used for the gas fill, the radiation energy reaches the wall in two distinct pulses (Fig. VII-7). The first pulse, from absorption in the radiation preheating layer just outside the fireball with emission of 4-10 eV x-rays, contains little energy (120 kJ) and produces a 3 kW/cm^2 flux at a four-meter radius first wall. Though this is done for a four-meter radius cavity, the same general results should apply to the three-meter case. The second, longer pulse (0.1 ms) is from radiation cooling of the whole gas once the fireball becomes optically thin. This pulse contains 17 times as much energy, produces a peak average wall flux of 10 kW/cm^2, and is composed mainly of 1-4 eV x-rays. The radiation front reaches the wall before the shock is driven outward into the cold gas by the higher pressure in the fireball. If we had included the high energy tail of the x-ray spectrum and the small fraction (< 1% of the beam energy) of Bremsstrahlung x-rays produced directly from beam target interactions, a third, much earlier pulse (at ~ 10 ns) would be seen.[7] These x-rays pass through the chamber gas without being absorbed; they penetrate into the wall and hence are less damaging to the surface.

Using a single group to represent radiation and the same initial conditions, similar simulations have been done at the University of Wisconsin.[4] These calculations do not observe the earlier, shorter pulse of x-rays. The

CALCULATION OF RADIATION EMISSION AT ALL FREQUENCIES YIELDS

→ X-RAY FLUX AT FIRST WALL

→ SHOCK OVERPRESSURE AT FIRST WALL

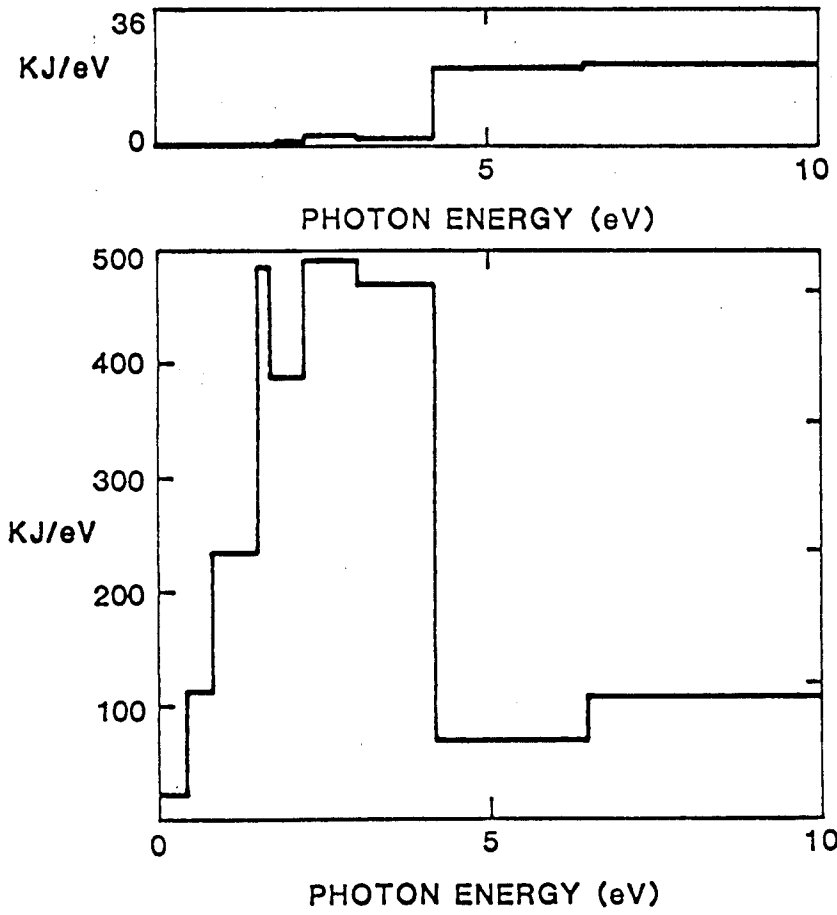

SHORT PULSE OF X-RAY ENERGY

- FROM ABSORPTION NEAR TARGET WITH EMISSION OF X-RAYS THAT REACH FIRST WALL
- <MAX>FLUX=3 kW/cm^2 AT 0.05 msec
- ENERGY=120 KJ
- PULSE LENGTH=0.02 msec

LONG PULSE OF X-RAY ENERGY

- FROM RADIATION COOLING OF WHOLE GAS
- <MAX>FLUX=10 kW/cm^2 AT 0.45 msec
- ENERGY=2 MJ
- PULSE LENGTH=0.1 msec

Fig. VII-7. The x-ray pulses seen at the four-meter first wall as a result of 23.5 MJ deposited in 50 torr, 750 K argon. The initial fireball size, 40 cm, corresponds to a 1 keV blackbody.

second, longer pulse produces roughly the same magnitude of flux as in the multigroup calculations, but occurs at about 0.1 ms rather than 0.45 ms. The fact that the single frequency group calculations do not produce the first pulse of x-rays is not of great consequence, because they only provide 6% of the radiated energy. Figure VII-7 shows that the later pulse is basically of a blackbody spectrum, which is the basic assumption in the single frequency group code. Thus the multifrequency group calculations seem to indicate that at a particular density of 10^{18} cm^{-3}, the single frequency group calculations are adequate for first wall design studies.

It is important to keep in mind that these quantitative results, obtained using both single group and multifrequency opacities, depend very strongly upon opacity values[25] for materials in the ground state. Calculations in this regime ($\lesssim$ 1 eV) are uncertain and mean free paths can be wrong by a factor of a hundred.[27] In addition, the conclusions obtained from these thermal transport simulations can depend strongly upon chamber radius, pellet yield, and the fractional distribution of the thermonuclear yield between the neutrons and the x-rays and ion debris; i.e. the 0.2% sodium case may not be the appropriate one to effectively protect the first wall if a different set of these parameters is envisioned.

If the gas density becomes lower, there will be more prompt x-rays getting through the gas and the spectrum of the radiated photons will less closely resemble a blackbody spectrum. There has been recent speculation that the cavity gas density may have to be reduced by an order of magnitude to allow the proper formation of beam channels. If this is the case, the single frequency group calculations may no longer be a valid treatment of the

fireball physics and multifrequency calculations may be required, especially to calculate the propagation of radiation out through the beam channels.

VII.E. Conclusions

We have presented calculations of fireballs propagating through a three-meter radius cavity filled with 1.8×10^{18} cm^{-3} argon, which has been seeded with various concentrations of sodium vapor. We have described the care which must be taken when considering the equation of state of a gas mixture and have shown that the opacity of argon to low energy photons can be greatly increased by the addition of small amounts of sodium. We have demonstrated that the variations in the opacity give us control over the radiant heat flux and overpressure on the first wall.

The case of 0.2% sodium is most closely studied as a candidate for the cavity gas, and it is found that the heat flux and overpressure are low enough that a first wall design seems probable. The design and the resultant mechanical and thermal stresses are discussed in detail in Chapter IX.

Finally, we have shown that, at a gas density of 1.8×10^{18} cm^{-3}, the single frequency group calculations adequately model the fireball propagation. At lower gas density, we expect that multifrequency calculations would become necessary.

References

1. R. W. Conn, "First Wall and Divertor Plate Material Selection of Fusion Reactors," J. Nucl. Mat. 76 & 77, 103 (1978).

2. G. Kulcinski, "First Wall Protection Schemes for ICF Reactors," J. Nucl. Mat. 85 & 86, 87 (1979).

3. R. W. Conn et al., "SOLASE, A Laser Fusion Reactor Study," University of Wisconsin Fusion Engineering Program Report UWFDM-220 (1978).

4. G. A. Moses et al., "The SOLASE Conceptual Laser Fusion Reactor Study," Proc. 3rd ANS Top. Meeting on Fusion Tech., 448.

5. S. I. Abdel-Khalik, G. A. Moses and R. W. Conn, "Engineering Problems of Laser Driven Fusion Reactors," Nucl. Tech. 43, 5 (1979).

6. D. L. Cook and M. A. Sweeney, "Design of Compact Particle Beam Driven Inertial Confinement Fusion Reactors," Proc. 3rd ANS Top. Meeting on Fusion Tech., 1178.

7. G. R. Magelssen, "X-Ray and Pressure Conditions on the First Wall of a Particle Beam Inertial Confinement Reactor," Bull. Amer. Phys. Soc. 24, 1071 (1979).

8. H. A. Bethe, "Theory of the Fireball," Los Alamos Scientific Laboratory Report LA-3046, (June 1964).

9. H. A. Bethe et al., "Blast Wave," Los Alamos Scientific Laboratory Report LA-2000, (March 1958).

10. G. I. Taylor, Proc. (London) Roy. Soc. A201, 159 (1950); A201, 175 (1950).

11. V. Zeldovich and Y. Raizer, Physics of Shock Waves and High Temperature Hydrodynamic Phenomena, Academic Press, I and II, New York (1966).

12. D. A. Freiwald and R. A. Axford, "Approximate Spherical Blast Theory Including Source Mass."

13. R. R. Peterson and G. A. Moses, "MFP - A Calculation of Radiation Mean Free Paths, Ionization and Internal Energies in Noble Gases," Computer Phys. Comm. 20, 353 (1980).

14. R. R. Peterson and G. A. Moses, "MIXER - A Multi-Species Optical Data and Equation of State Computer Code," University of Wisconsin Fusion Engineering Program Report UWFDM-372, (Sept. 1980).

15. G. A. Moses and R. R. Peterson, "First Wall Protection in Particle Beam Fusion Reactors in Inert Cavity Gases," Nuclear Fusion 20, 849 (1980).

16. R. R. Peterson, G. W. Cooper and G. A. Moses, "Cavity Gas Analysis for Light Ion Beam Fusion Reactors," University of Wisconsin Fusion Engineering Program Report UWFDM-371, August (1980) (to appear in Nuclear Technology).

17. G. W. Cooper, R. R. Peterson and G. A. Moses, Proc. 1980 IEEE International Conf. on Plasma Science, Madison, Wisconsin, 25, May 19-21, (1980).

18. R. R. Peterson and G. A. Moses, "Blast Wave Calculations in Argon Cavity Gas for Light Ion Beam Fusion Reactors," University of Wisconsin Fusion Engineering Program Report UWFDM-315, (October 1979).

19. G. A. Moses et al., "First Wall and Cavity Design Studies for a Light Ion Beam Driven Fusion Reactor," University of Wisconsin Fusion Engineering Program Report UWFDM-320, (September 1979).

20. M. A. Sweeney, Particle Beam Fusion Progress Report, July-December 1979, SAND80-0974; M. A. Sweeney and D. L. Cook, Bull. Amer. Phys. Soc. 24, 1071 (1979).

21. M. A. Sweeney, Particle Beam Fusion Progress Report, October 1977 - March 1978, SAND79-0002, 58; D. L. Cook and M. A. Sweeney, Proc. 3rd Topical Meeting on the Technology of Controlled Nuclear Fusion, Santa Fe, NM, May 9-11, (1978), (NAS, 1978), 2, 1178.

22. M. A. Sweeney and D. L. Cook, Proc. Topical Meeting on Inertial Confinement Fusion, San Dieg, CA, February 26-28, 1980 (Optical Society of America, 1980), 18.

23. R. L. Engelstad and E. G. Lovell, "First Wall Mechanical Design for Light Ion Beam Fusion Reactors," University of Wisconsin Fusion Engineering Program Report UWFDM-322, (December 1979).

24. L. Baker, Sandia Laboratories Report SAND79-0386, March 1979. The code described, CHARTB, is an MHD version of CHARTD [S. L. Thompson, Sandia Laboratories Report SLA-73-0477, October 1973], which contains a multigroup, flux limited diffusion package and is also used for plasma channel computations.

25. W. F. Huebner, A. L. Merts, N. H. Magee and M. F. Argo, Multifrequency Opacity Data Obtained from LASL Group T4; cf. Los Alamos Scientific Laboratory Report LA-6760-M, (August 1977).

26. D. L. Cook and M. A. Sweeney, J. Nucl. Mat. 85, 127 (1979).

27. W. F. Huebner, private communication.

VIII. First Wall Mechanical Response

VIII.A. General Design Considerations

One of the major influences on the mechanical design of the TDF first wall is the shock wave generated by the fireball. The associated heat flux is also a key issue and is considered in the following chapter. The shock wave effectively imparts a dynamic pressure to the first wall and should be rather uniformly distributed over the surface. If the first wall structure is modeled as a perfect isolated thin cylindrical shell, then the radial pressure distribution will be sustained by uniform circumferential normal stress. In other words, such a concept is essentially a thin-walled tube in which the pressure generates "hoop stresses" and complimentary axial normal stresses. Accounting for distributed mass and elasticity for this model will lead to dynamic response characterized by a "breathing mode" in which each cross section remains circular, expanding and contracting in simple harmonic motion following the mechanical shock.

However, such a representation is quite idealized. The inevitable presence of external constraints in a practical design would preclude this type of behavior. Structural supports, diagnostic entries, beam ports, etc., will result in flexural stress in the wall under pressure loading. Thus, since flexural stress will be developed, a more realistic approach appears to be a design in which flexural response is the basis for the modeling. A component of the first wall is viewed as a flexural plate element appropriately supported at some orientation and distance from the cavity center. The essential difference in the load carrying mechanisms for these two models is shown in Fig. VIII-1. In the tube model, circumferential curvature and free expansion allow for the development of uniform hoop stresses as reactions

Figure VIII-1

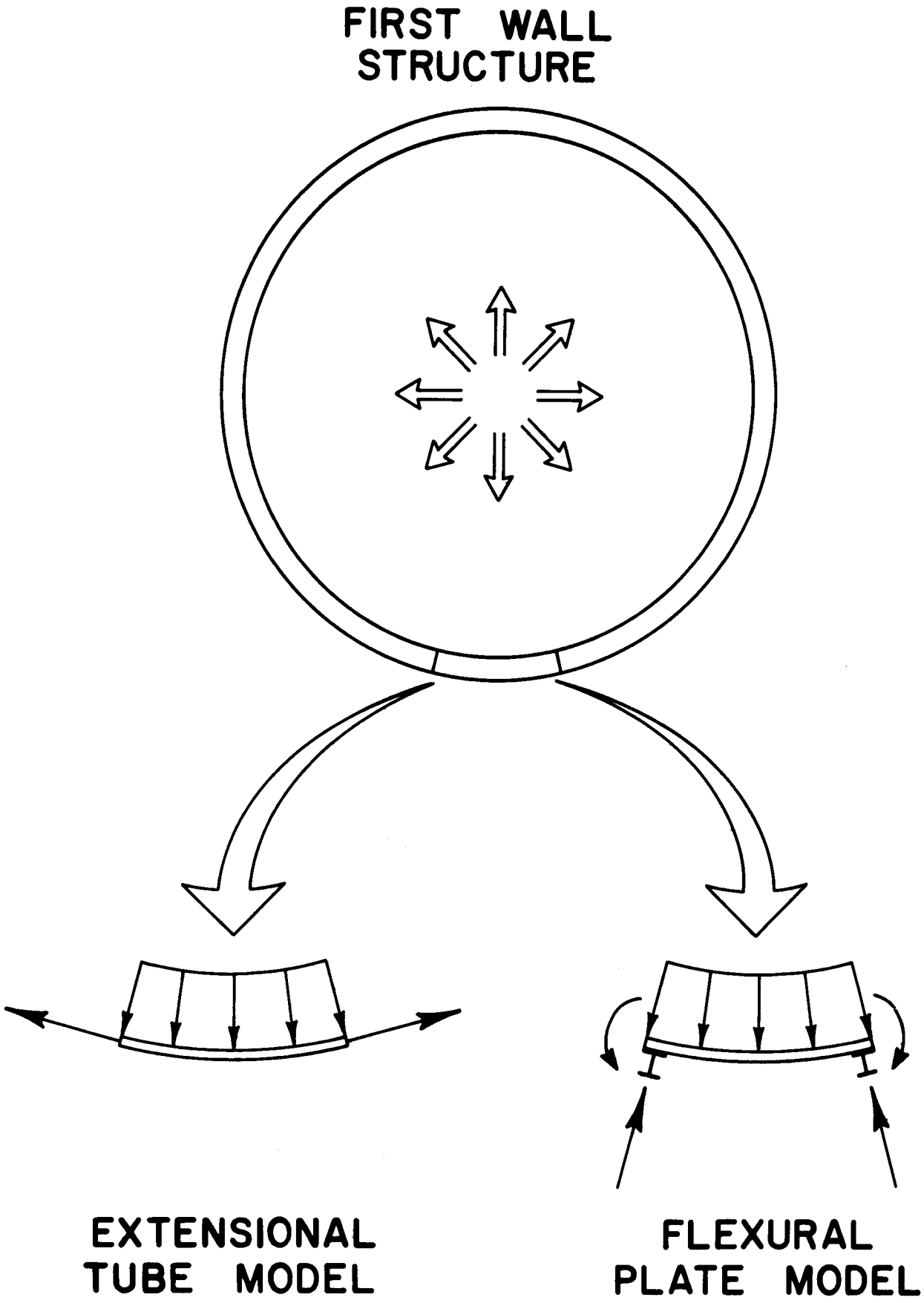

to the loading. If portions of the wall are restricted from expanding, the displacements are nonuniform. Flexural moment and transverse shear are developed as reactions to the pressure with radial forces transmitted into a secondary structural system. The resulting bending stresses vary throughout the plate in the radial, circumferential and axial directions.

The secondary structure can be based upon a number of systems. However, since the overall shape of the TDF is cylindrical, a configuration of axial stringers and circumferential ribs is a basic functional support system. A typical section is shown schematically in Fig. VIII-2. While the vertical stringers would directly support the plates, the ribs could either provide the same direct support or be offset, encircling the stringers and contacting only them. The latter design would be advantageous in a situation where it is necessary to actively cool the wall, e.g., with flow over the back surface. In this case the stringers will respond as structural beams while the ribs function to carry the "hoop forces."

It should also be noted that a single plate may span a number of stringers and perhaps all of the ribs if appropriate. A system of this type lends itself well to the development of a modular design both for the target development facility and a conceptual reactor. Individual module size would depend upon additional factors such as maintenance, beam line characteristics, etc.

Although the first wall of the proposed TDF is solid, a more efficient component may be necessary in reactor applications. For example, a hollow cellular plate, shown in Fig. VIII-3, can provide a flexural stiffness and strength much higher than a solid unit of comparable mass when subjected to transverse loading. In addition to these mechanical advantages, it would also

Figure VIII-2

CONCEPTUAL FIRST WALL SUPPORT STRUCTURE

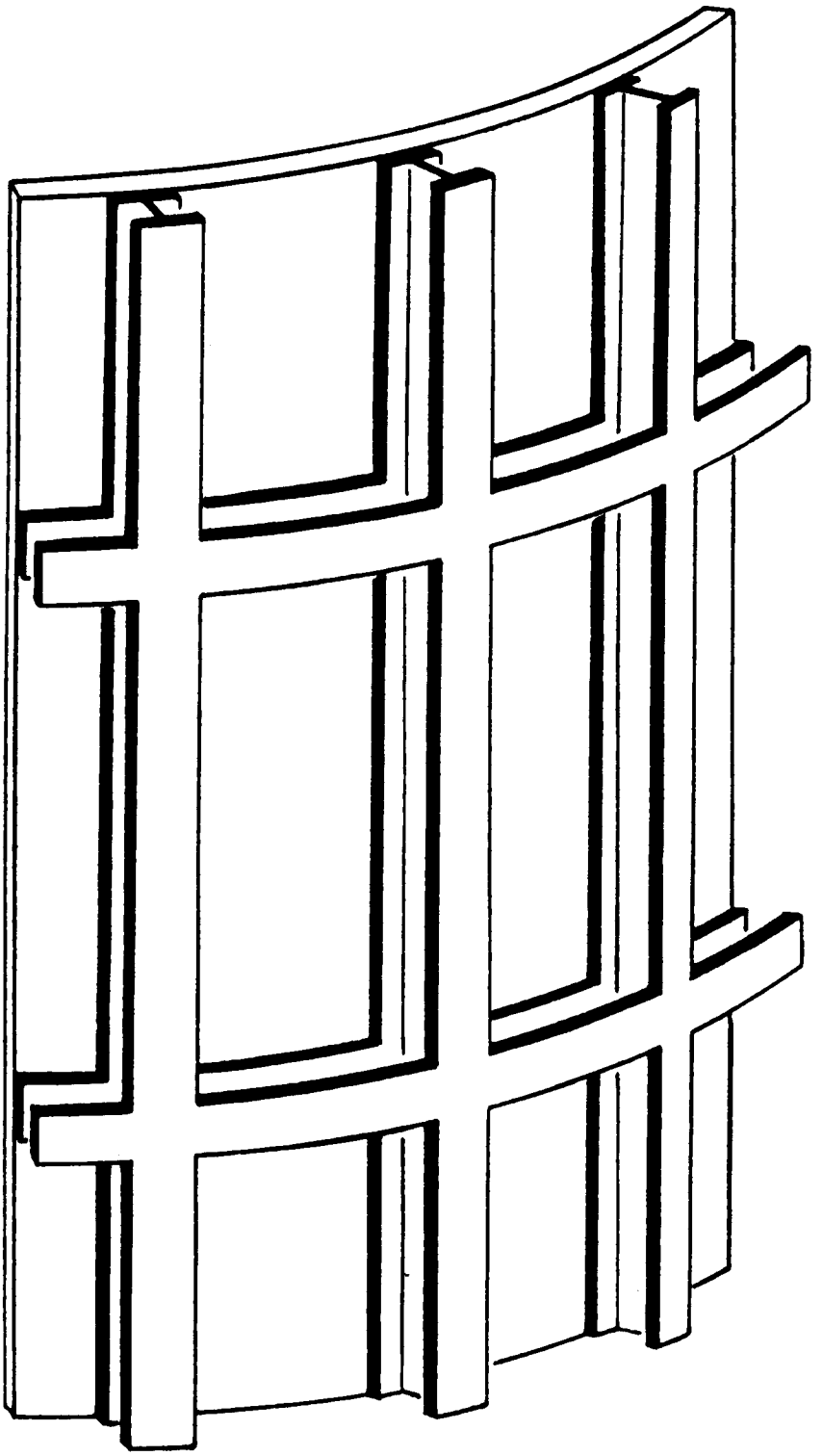

Figure VIII-3

CELLULAR WALL IN DYNAMIC FLEXURE

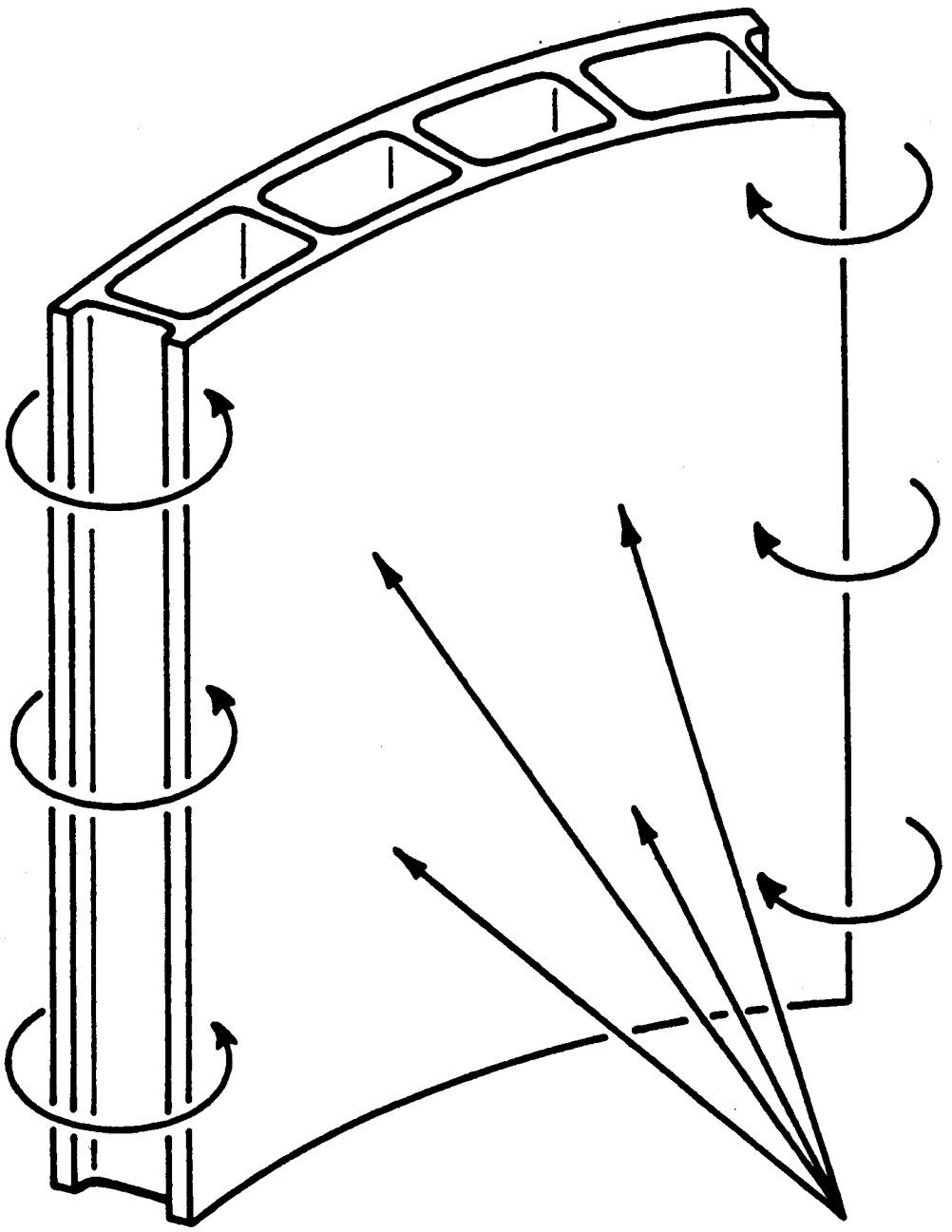

be well suited for coolant flow through internal channels and offers a minimum material thickness to neutrons for the promotion of adequate tritium breeding in the blanket behind it.

Other variations in wall design details are possible. Individual plates can be flat as previously indicated or they could be formed with the curvature of the first wall centerline. The cavity radius is much larger than the plate span, i.e. the horizontal distance between stringers. This implies a very shallow curved panel which for most practical purposes can be treated as flat. The differences in mechanical response between these two geometries should not be significant.

On the other hand, if swelling or mean thermal strains become appreciable and they are restricted by geometric constraints, substantial circumferential stresses may be generated with subsequent buckling or other structural degradation. Thus, it may be necessary to modify the proposed basic design to accommodate such effects. An expansion joint system at the stringer support locations would be one possiblity. A simpler design can be based upon individual panels produced with additional curvature and the assemblage forming a "scalloped" first wall configuration. Induced strains would change the curvature slightly without generating large forces. A corrugated or creased panel would serve a similar purpose, i.e., permitting material dimensional changes without creating significant stresses. Whether concave or convex scalloping is more adantageous remains to be determined. Figure VIII-4 shows configurations for this scheme which is a preliminary concept at this point.

VIII.B. Plate Mechanical Analysis

First wall response analysis for mechanical shock loading requires specification of a number of mechanical characteristics. These include

Figure VIII-4

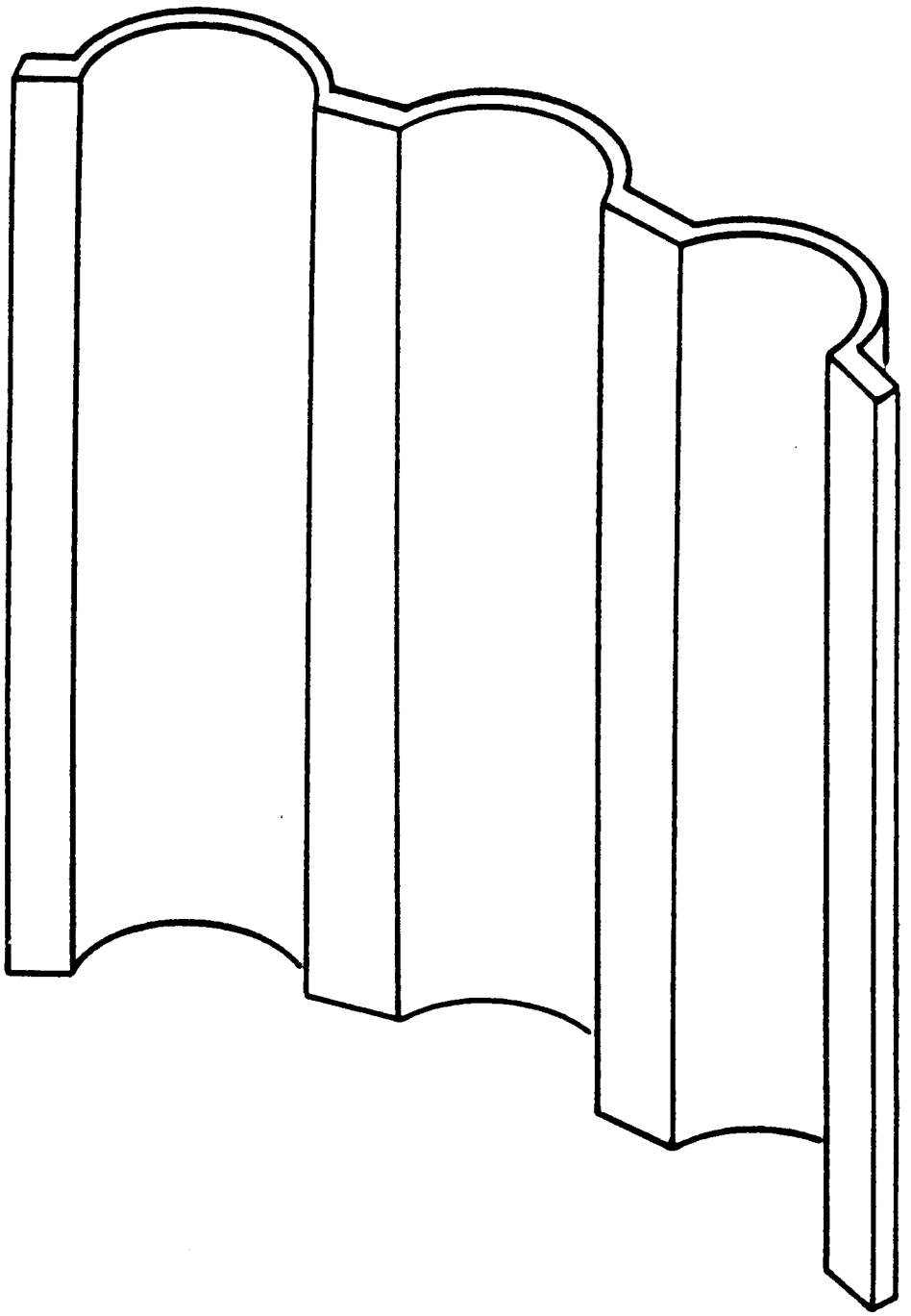

SCALLOPED WALL CONCEPT

identification of plate support conditions. At a supporting beam (e.g., stringer), it is assumed that a plate edge is very substantially constrained by the joint or connection. The geometric conditions implied by this are essentially the same as for a continuous plate spanning many beams at those locations where it bridges such supporting members, i.e. rotations and relative edge deflections are negligible. Thus the unit analyzed is a rectangular plate with so-called "clamped" or "built-in" edges all around. This may be a single plate or it may be a subdivision of a large plate supported by a number of ribs and stringers.

Radial pressure applied to the plate surface facing the cavity produces circumferential normal stresses which are tensile at the edges and compressive at the center. Axial normal stresses would vary in a similar manner in the vertical direction. These flexural stresses are linear functions through the thickness with equal but opposite values on the outside surface of the plate. The relative side dimensions of the plate (aspect ratio) affect the magnitudes of these stresses. Typical results are shown in Fig. VIII-5 for static uniform pressure. As expected, extreme stresses are minimized for a square plate. Stresses vary as the relative side dimensions change but quickly approach constant values for aspect ratios greater than two. (It also follows that for aspect ratios greater than two, the boundary conditions on the short sides do not influence maximum stresses.) Since these limiting magnitudes are not significantly greater than the minima, they can be conveniently used for design purposes.

The dynamic analysis of the plate components can be developed by determining the quasi-static response and multiplying it by a dynamic load factor (DLF), or more descriptively a dynamic load function, to give the

Figure VIII-5

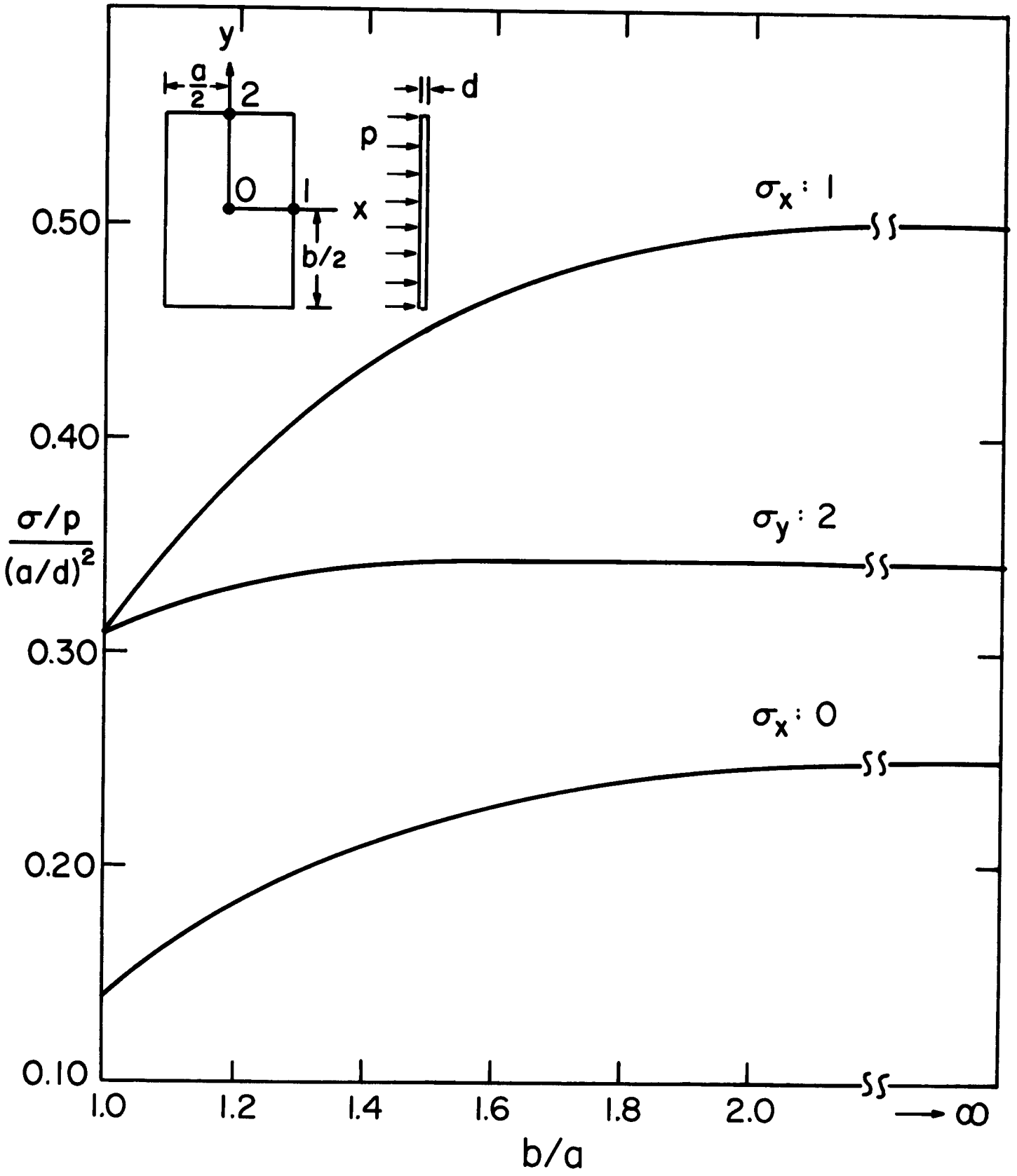

DIMENSIONLESS STATIC STRESS VS. ASPECT RATIO

corresponding response. Deflections and stresses are proportional and therefore the dynamic load factor may be used in either case. Under uniform impulsive pressure, plate response can be represented by a single degree of freedom system and thus the results for this model can be used to simplify the dynamic analysis. For example purposes, consider a linear undamped system with effective mass m and stiffness K. If x denotes displacement and the excitation (force) is F(t), a function of time, the basic equation for motion is

$$m\ddot{x} + Kx = F(t)$$

in which ($\cdot$) represents a time derivative. Let x_0, $\dot{x}_0$ and ω be the original displacement, velocity and natural frequency, respectively. Defining $F(t) = F_{max} f(t)$, the static response is

$$x_s = F_{max}/K = F_{max}/m\omega^2 \quad .$$

Thus the complete solution may be expressed as

$$x = x_0 \cos \omega t + (\dot{x}_0/\omega) \sin \omega t + x_s \omega \int_0^t f(\tau) \sin \omega(t - \tau)\, d\tau \quad .$$

Here τ is simply a time integration variable. To continue the example, a particular loading function will be specified. The pressure pulse for many cases can be adequately represented by a ramp with rise time t_r followed by an exponential decay as shown in Fig. VIII-6.

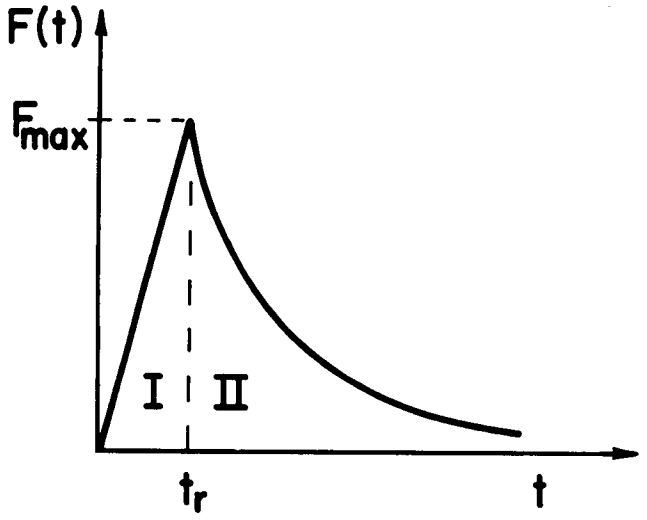

Interval I:

$$\tau \leq t_r \qquad f(\tau) = \frac{\tau}{t_r}$$

Interval II:

$$\tau > t_r \qquad f(\tau) = e^{-k(\tau - t_r)}$$

Figure VIII-6

For the first interval the initial velocity and displacement are zero. Then the corresponding response is

$$x = (x_s/\omega t_r)[\omega t - \sin \omega t] \qquad t < t_r \quad .$$

It follows that

$$DLF = (\omega t - \sin \omega t)/\omega t_r \quad .$$

For the second interval the initial values x_0 and $\dot{x}_0$ are determined from the preceeding results. With these and the exponential loading function, the response leads to a corresponding dynamic load factor for $t > t_r$:

$$DLF = \left[\frac{k^2/\omega^2}{1 + k^2/\omega^2} - \frac{\sin \omega t_r}{\omega t_r}\right] \cos \omega(t - t_r)$$

$$+ \left[\frac{k/\omega}{1 + k^2/\omega^2} + \frac{1 - \cos \omega t_r}{\omega t_r}\right] \sin \omega(t - t_r)$$

$$+ e^{-k(t-t_r)}/(1 + k^2/\omega^2) \qquad t > t_r \quad .$$

In general a number of computations are made to obtain design data. Natural frequencies are calculated as a function of plate geometry terms. Then the dynamic load factor is determined as a function of time for various frequencies and excitation parameters k and t_r and the maximum values are identified. Static deflections and stresses are then multiplied by the maximum DLF to produce maximum dynamic deflections and stresses. The general

procedure and details can be found in University of Wisconsin Fusion Engineering Program Report UWFDM-322.

VIII.C. Specific Response Results

With the analysis of UWFDM-322 as a basis, a computer code, PSHAKE, has been developed for the determination of frequencies, dynamic stresses and deflections for solid and hollow plates of various materials subjected to general time-dependent pressure loadings. This program has also been coupled with the thermal stress code discussed in Chapter IX to produce the total stress history in a first wall plate component.

Results presented here are for a solid ferritic steel (HT-9) plate having a height, width and thickness of 200, 47.12 and 5 cm, respectively. The shock pressure data from the fireball code is represented analytically to determine dynamic load factors as described in the previous section. The data used for this calculation are given in Table VIII-1. The fundamental frequency of this component in flexure was found to be 1154 Hz. Figure VIII-7 shows the circumferential normal stress profile across the horizontal midline of the cavity side of the plate for a 200 MJ target yield. This distribution occurs during the first cycle of motion when the plate experiences its maximum outward radial displacement. The extreme tensile and compressive stresses are 66.4 MPa and 33.2 MPa, respectively. For the same case the circumferential stress history is shown in Fig. VIII-8 for a point at the center of the plate surface facing the cavity. Note that compressive stress is plotted above the axis with peak value corresponding to the midspan amplitude of Fig. VIII-7. This point was chosen for study since compressive thermal stress from the heat flux will add directly whereas flexural and thermal stress will counteract each other near the edges. The analytical form of the pressure pulse is

Table VIII-1

Data for Mechanical Response Calculations

Cavity Radius	3 m
Wall Panel Dimensions	
height	200 cm
width	47.12 cm
thickness	5.0 cm
aspect ratio	4.24
Wall Panel Material	Ferritic Steel (HT-9)
Energy in Fireball	60 MJ
Analytic Dynamic Pressure Parameters	
maximum overpressure	1.126 MPa
t_r	0.075 msec
k	3000 sec^{-1}
maximum dynamic load factor	1.328

Figure VIII-7

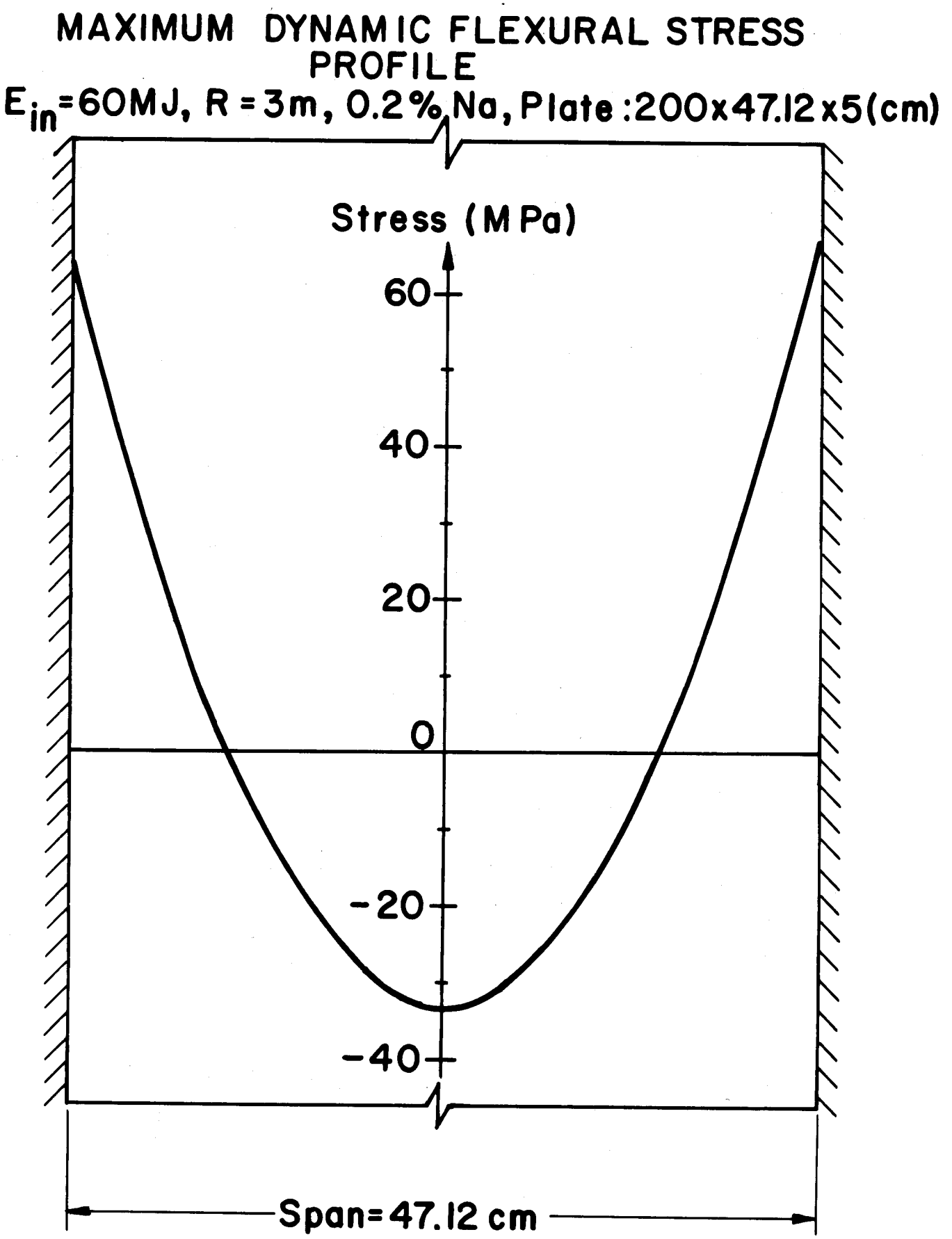

Figure VIII-8

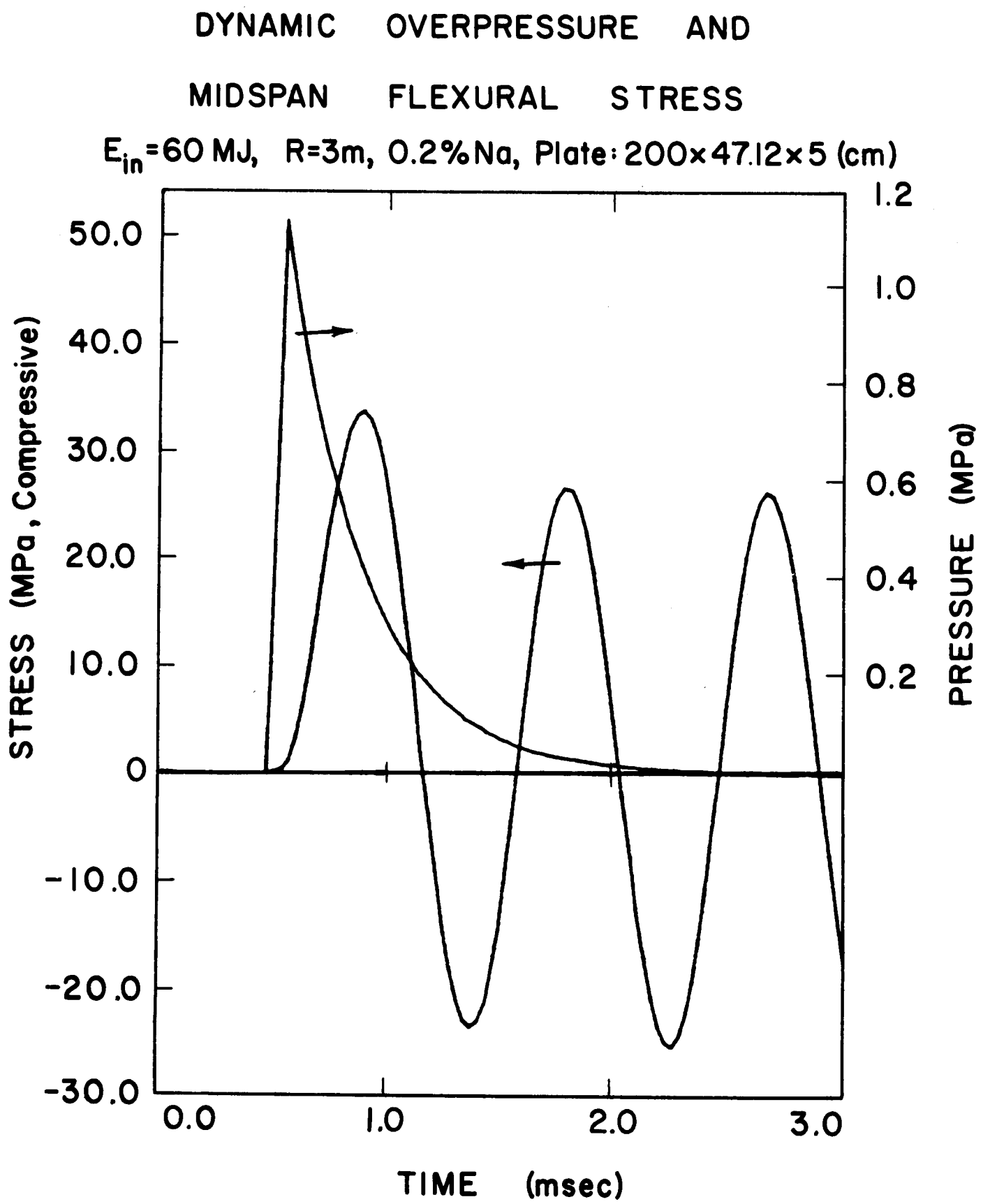

superimposed to show its influence upon the response. It can be seen that initially the stress response follows the pulse and subsequently develops into free vibration. (Damping has not been included in these calculaions but is currently being added to the program.) Also, the time history of transverse displacement will correspond directly with that of stress. The maximum displacement in this example is 0.013 cm.

In this case the flexural stress amplitude is rather moderate. This is a result of the design parameters (i.e. plate dimensions) that have been chosen. However, when it is combined with thermal stress, sizeable values can be produced. The net effect of these two components will be shown in the next chapter and the result used as the basis for fatigue life determination.

IX. First Wall Thermal Response

IX.A. Introduction

The generation of thermal stresses in ICF reactor first walls is a critical issue in cavity design.[1,2] There may be large amounts of heat absorbed at the inner surface of the cavity first wall over very short periods of time. The magnitudes of the wall temperature gradients, and thus the thermal stresses, depend upon the characteristics of the surface heat pulse as well as the first wall geometry and material. As discussed in Section VII, the cavity gas in the light ion beam target development facility has a large effect on the pulse of thermal radiation incident on the cavity first wall. By adjusting the composition of the cavity gas, the thermal stresses in the first wall may be controlled. In addition, by choosing a first wall material with high conductivity and/or a low thermal expansion coefficient the thermal stresses can be minimized. Also, a material with a large fatigue lifetime is desirable.

Accompanying the thermal stresses are flexural stresses caused by the large overpressure of the shock wave which hits the first wall. The details of these mechanically induced stresses are discussed in Chapter VIII. The time of occurrence of the thermal stresses may be adjusted relative to the flexural stresses by tailoring the radiative properties of the cavity gas so that the total stresses are minimized.

In this chapter, we describe the model used in the evaluation of the thermal stresses. This model is incorporated in the TSTRESS computer code. The accuracy of the numerical solution in TSTRESS is tested by comparison with a problem with an analytical solution. Finally, representative thermal

stresses are presented with the corresponding flexural stresses for various choices of the cavity gas discussed in Chapter VII.

IX.B. Model and Computer Code Development

In the TSTRESS code we use a thermal stress model which is valid for flat plates which are allowed to expand under heating. In this model, differential expansion creates compressive stresses in the hotter sections of the plate.

In addition to differential expansion, we consider three other contributions to the transient stresses in the plate; swelling, irradiation creep and flexural stresses. The flexural stresses are discussed in Chapter VIII and will not be described in detail here. Swelling is caused by the formation of voids in the material due to the fusion generated 14 MeV neutrons and adds to thermal expansion. Irradiation creep is a deformation of the material which tends to reduce the stresses in a material. It occurs when atoms are knocked from their lattice points when the material is under a stress.

Including the effects of thermal expansion, swelling and irradiation creep, the equation of expansion is written as

$$\frac{1}{\ell}\frac{d\ell}{dt} = [\alpha\dot{T} + \frac{1}{3}S(z)] - \frac{1}{2}\psi(z) \qquad \text{(IX-1)}$$

where ℓ is a unit of length in the direction perpendicular to the plane of the plate (the z-direction), $\alpha(z)$ is the coefficient of thermal expansion, S the swelling rate and $\psi(z)$ the creep rate.

The differential expansion causes thermal stresses in the plane of the plate (x-y plane). The equations governing the x and y components of the thermal stress are

$$\frac{\partial}{\partial t}\ \sigma_x(z) = \frac{1}{h}\int_0^h \frac{1+\nu}{1-\nu}\,2\mu\,[\alpha\dot{T}(z') + \frac{1}{3}\dot{S}(z')]\,dz' - \frac{1+\nu}{1-\nu}\,2\mu\,[\alpha\dot{T}(z)$$

$$+ \frac{1}{3}\dot{S}(z)] + \frac{1}{h}\int_0^h \frac{\mu}{1-\nu}\,\psi(z')\,[(2-\nu)\,\sigma_x(z') - (1-2\nu)\,\sigma_y(z')]\,dz' \qquad \text{(IX-2)}$$

$$- \frac{\mu}{1-\nu}\,\psi(z)\,[(2-\nu)\,\sigma_x(z) - (1-2\nu)\,\sigma_y(z)]$$

and

$$\frac{\partial}{\partial t}\,\sigma_y(z) = \frac{1}{h}\int_0^h \frac{1+\nu}{1-\nu}\,2\mu\,[(\alpha\dot{T}(z') + \frac{1}{3}\dot{S}(z')]\,dz' - \frac{1+\nu}{1-\nu}\,2\mu\,[\alpha\dot{T}(z)$$

$$+ \frac{1}{3}\dot{S}(s)] + \frac{1}{h}\int_0^h \frac{\mu}{1-\nu}\,\psi(z')\,[(2-\nu)\,\sigma_y(z') - (1-2\nu)\,\sigma_x(z')]\,dz' \qquad \text{(IX-3)}$$

$$- \frac{\mu}{1-\nu}\,\psi(z)\,[(2-\nu)\,\sigma_y(z) - (1-2\nu)\,\sigma_x(z)]\ .$$

Here h is the width of the plate, μ is the shear modulus and ν is Poisson's ratio. μ, α, and ν may only be weak functions of position or there would be terms in the derivatives of these parameters which would have to be added to Eqns. IX-2 and IX-3.

In the model we have chosen, the membrane loads in the x and y directions,

$$N_x = \int_0^h dz\ \sigma_x(z,t) \qquad \text{(IX-4)}$$

and

$$N_y = \int_0^h dz\ \sigma_y(z,t) \qquad \text{(IX-5)}$$

are constant in time. This conservation of membrane load is tested in the thermal stress code TSTRESS[3] by comparing N_x and N_y calculated for current stresses with those calculated at the beginning of the problem.

TSTRESS uses a finite difference method to calculate the transient thermal stresses in the plate for given time-dependent temperature profiles. The accuracy of TSTRESS has been tested by running a sample problem which has a known analytic result. This test problem involves the thermal creep relaxation of a linear residual stress distribution through a flat plate. There are no membrane forces imposed (N_x=0, N_y=0) and swelling and irradiation creep are ignored. The creep law is chosen as

$$\dot{\varepsilon}^c_{eq} = A\ \sigma^4_{eq} \qquad \text{(IX-6)}$$

where

$$A = 1.5 \times 10^{-14}\ hr^{-1} - ksi^{-4} \quad . \qquad \text{(IX-7)}$$

The initial linear residual stress profile is established by putting a time independent linear temperature profile across the plate. The initial stresses are then

$$\sigma_x = \sigma_y = \frac{2\alpha(1+\nu)\nu\Delta T z}{(1-\nu)h} \qquad \text{(IX-7)}$$

where ΔT is temperature difference across the plate.

As time advances the stresses for this problem may be written analytically as

$$\sigma_x(z,t) = [3BAt + \sigma_x(z,t=0)^{-3}]^{-1/3} \qquad \text{(IX-8)}$$

and

$$\sigma_y(z,t) = [3BAt + \sigma_y(z,t=0)^{-3}]^{-1/3} \qquad \text{(IX-9)}$$

where

$$B = \mu \left(\frac{1+\nu}{1-\nu}\right) . \qquad \text{(IX-10)}$$

Figure IX-1 shows a calculation of these stresses done by TSTRESS. Here, we have used the parameters

$$\alpha = 9.5 \times 10^{6}\ K^{-1}$$

$$\mu = 1.5711 \times 10^{4}\ \text{ksi}$$

$$\nu = 0.33$$

$$h = 5.0\ \text{cm}$$

$$\Delta T = 200\ K \quad .$$

These calculations show excellent agreement between analytic and TSTRESS results.

Figure IX-1

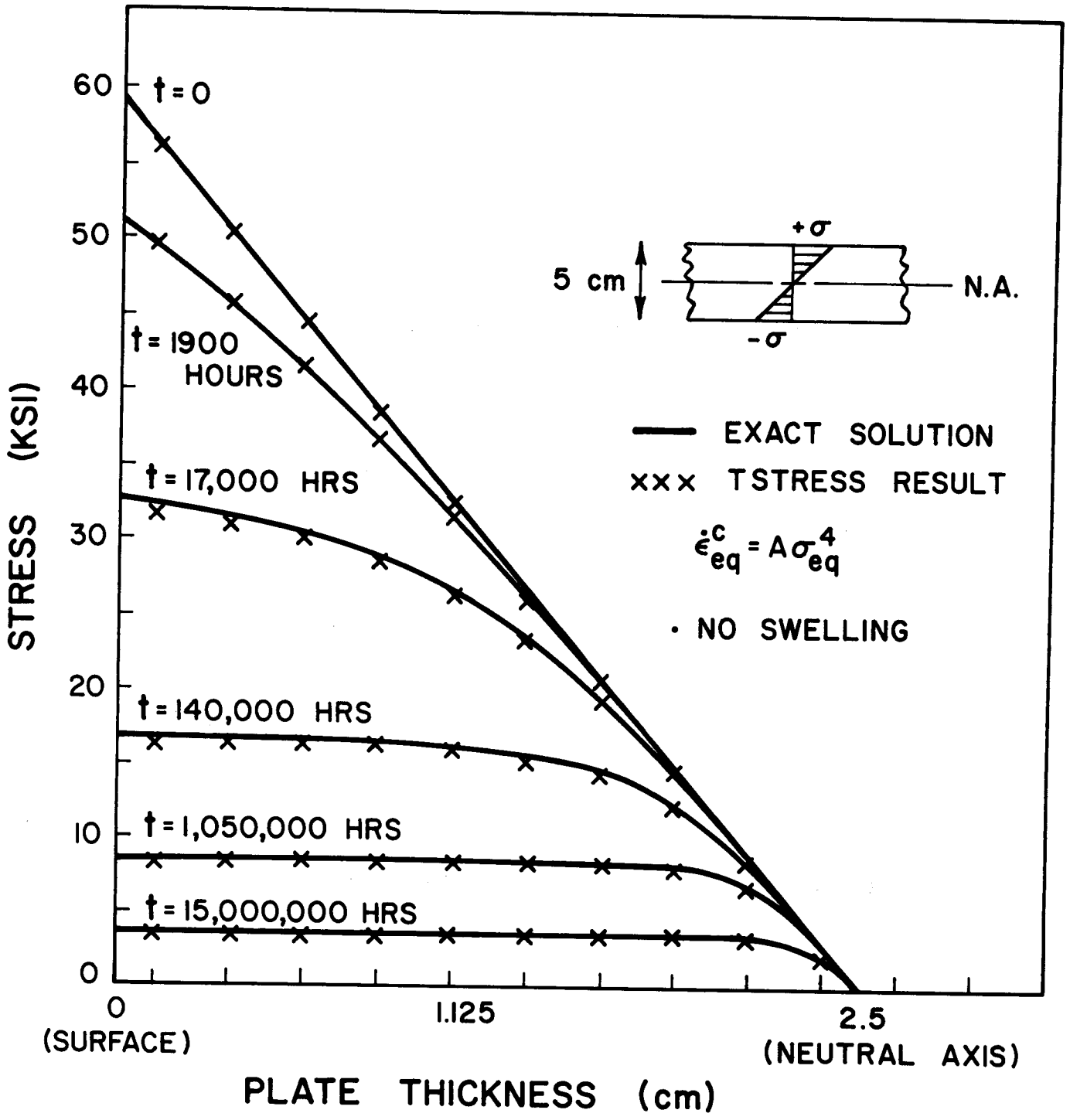

CREEP RELAXATION OF A LINEAR RESIDUAL STRESS DISTRIBUTION

IX.C. Stresses in TDF

Using TSTRESS, the thermal stresses in the first wall of the Target Development Facility (TDF) have been calculated. The fluxes of radiant heat on the first wall discussed in Chapter VII and a simple temperature diffusion code are used to calculate the temperature profiles. The wall has been assumed to be a solid plate 5 cm thick, made of HT-9 and cooled at its back surface to 300 K. For each choice of cavity gas composition we have calculated the thermal stresses in this wall.

The absolute magnitude of the thermal stresses is not the only issue because the relationship between the thermal stresses and the flexural stresses discussed in Chapter VIII is also important. The thermal stresses are strongly compressive in a narrow layer at the front of the plate and weakly tensile in the remainder of the plate while the flexural stresses oscillate in time between equal compressive and tensile values. At the center of the front face of a plate with clamped edges, the flexural stresses begin as compressive while they are 180° out of phase at the clamped edges. Since the absolute values of the flexural stresses should reach a maximum during the first oscillation, the greatest total stress should occur at the center of the front face.

In Figs. IX-2 to IX-4, we show the thermal, flexural and total stresses at the center of the front face of a plate of HT-9 with clamped edges. The stresses are taken to be positive when they are compressive. Plate parameters are given in Table IX-1. These plots are for cavity gas compositions of pure argon, 0.2% sodium and 2.0% sodium impurity concentrations. The argon density is 1.8×10^{18} cm^{-3} and the pellet yield is 100 MJ with 30 MJ in the x-rays and ion debris. It is clear that the worst case corresponds to 0.2% sodium with a

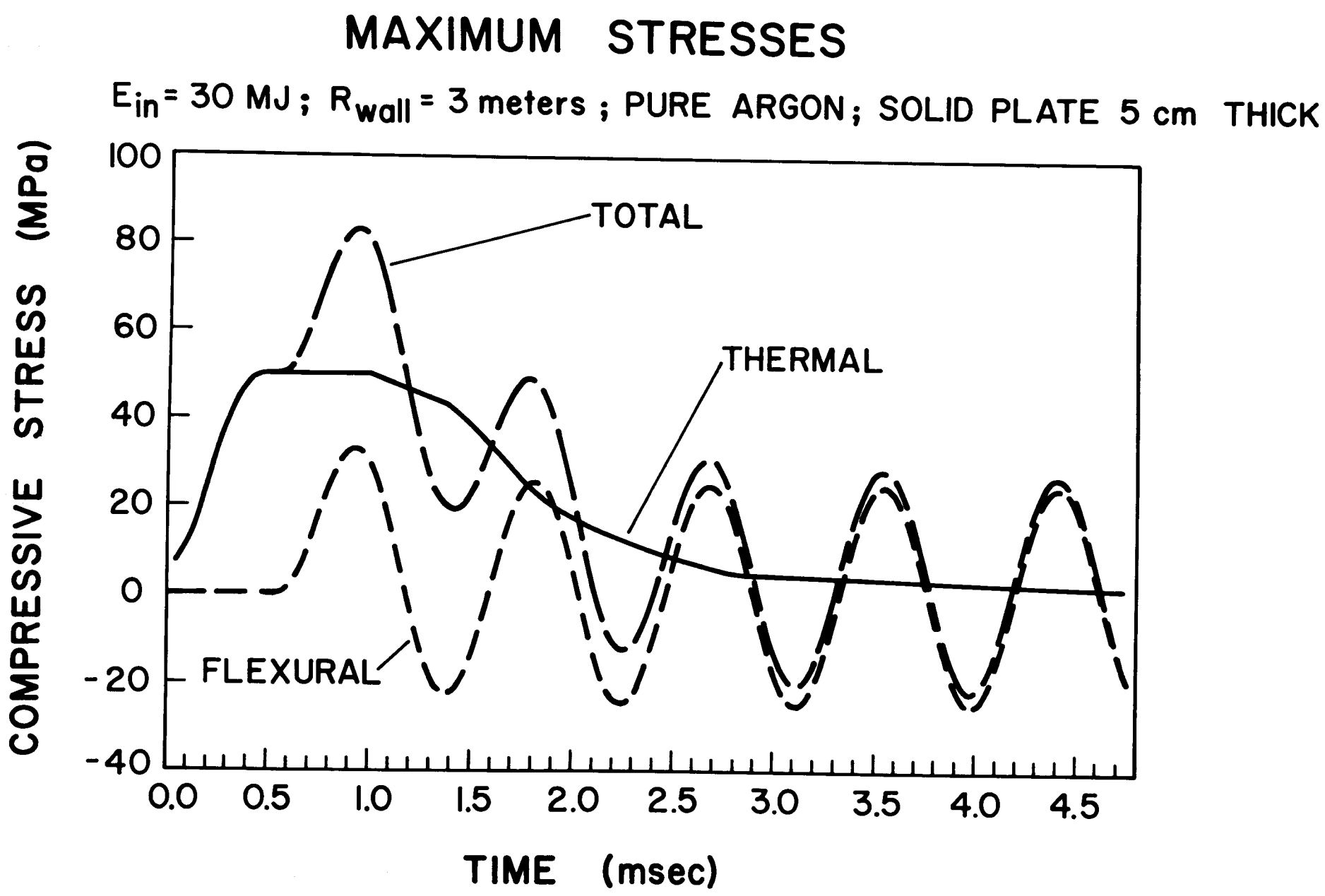

Figure IX-2. Thermal, flexural and total compressive stresses at the front face center. Plate thickness = 5 cm, E_{fusion} = 100 MJ, R_{wall} = 3 meters, pure argon, HT-9.

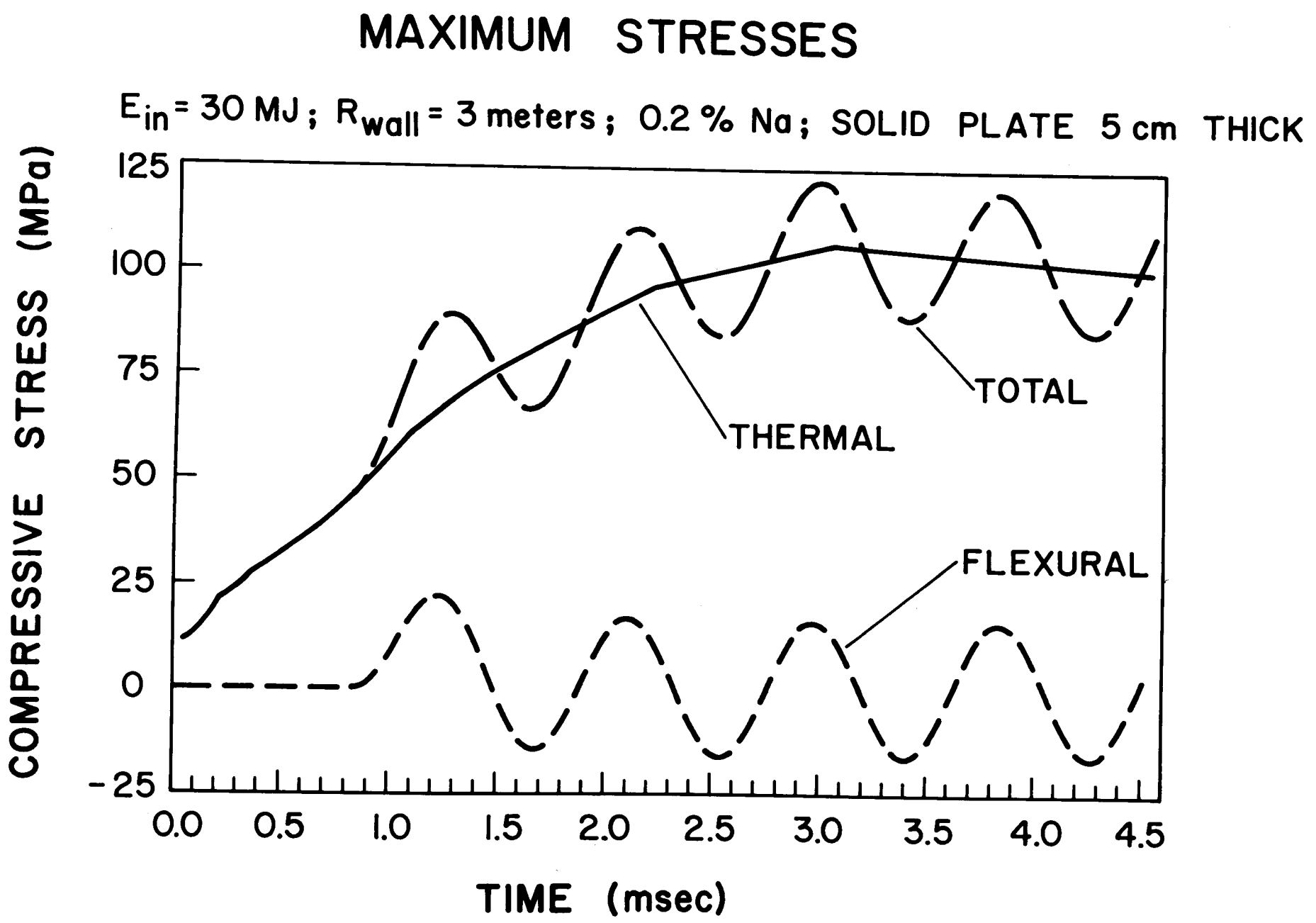

Figure IX-3. Thermal, flexural and total compressive stresses. Same case as Fig. IX-2 except cavity gas contains 0.2% Na.

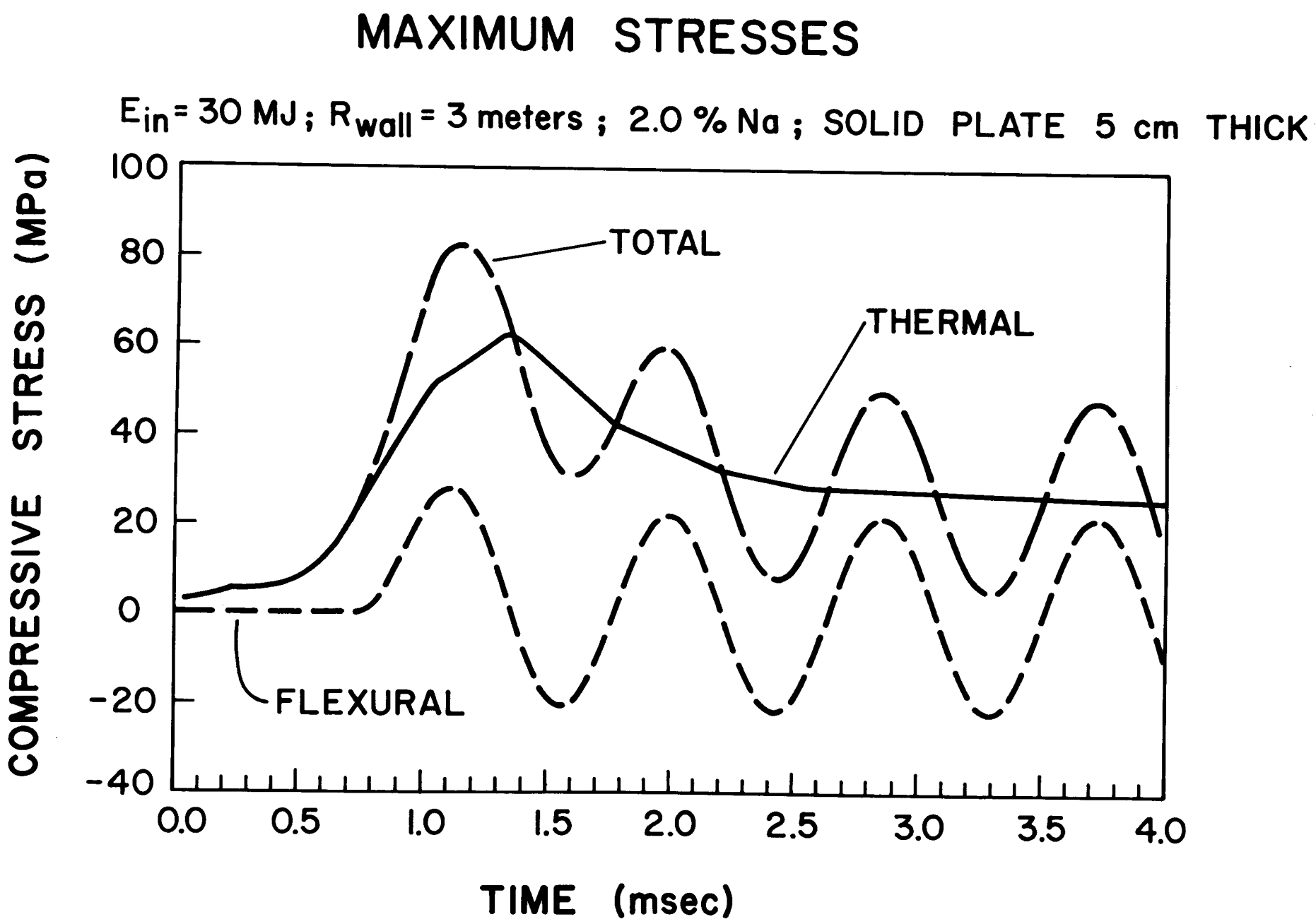

Figure IX-4. Thermal, flexural and total compressive stresses. Same case as Fig. IX-2 except cavity gas contains 2.0% Na.

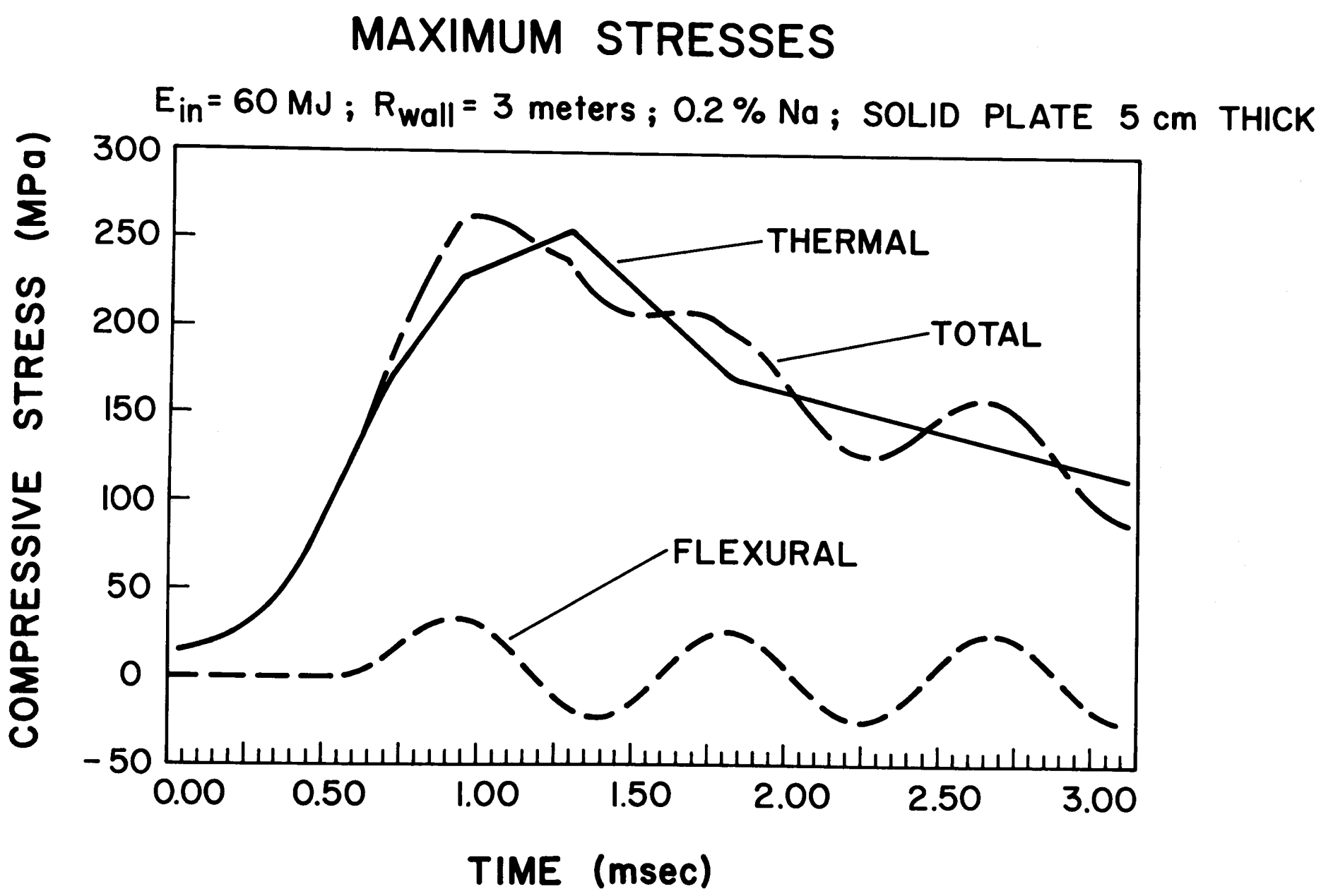

Figure IX-5. Thermal, flexural and total compressive stresses. Same case as in Fig. IX-3 except E_{fusion} = 200 MJ.

Table IX-1

Panel axial height	2 m
Panel span	0.47 m
Panel thickness	0.05 m
Reactor height	6 m
Chamber radius	3 m
First wall material	HT-9
First wall type	solid

maximum total stress of 125 MPa. This compares favorably with an allowable maximum of 420 MPa, a limit from HT-9 fatigue data for 5×10^4 cycles.

A calculation has also been done for a 200 MJ target yield in the TDF cavity filled with argon with a 0.2% sodium impurity. This calculation, whose time dependent stresses are shown in Fig. IX-5, predicts a maximum total stress of ~250 MPa. This is again less than the allowable 420 MPa set by the fatigue lifetime of the wall.

These results offer confidence that the first wall can survive the effects of thermal stresses. The worst case scenario with 200 MJ of fusion yield, 60 MJ total in x-rays and ion debris, and 0.2% sodium concentration in the cavity gas did not exceed the stress criteria for a fatigue lifetime of 5×10^4 shots.

References

1. R.W. Conn, et al., "SOLASE, A Conceptual Laser Fusion Reactor Design," University of Wisconsin Fusion Engineering Program Report UWFDM-220 (December 1977).

2. R.W. Conn, et al., "SOLASE-H, A Laser Fusion Hybrid Study," University of Wisconsin Fusion Engineering Program Report UWFDM-270 (May 1979).

3. R.R. Peterson, R.D. Watson, W.G. Wolfer and G.A. Moses, "TSTRESS - A Thermal Stress Computer Code," University of Wisconsin Fusion Engineering Program Report UWFDM-382 (December 1980)

X. First Wall and Cavity Design

X.A. Introduction

The first wall and cavity of the Target Development Facility (TDF) are expected to experience the same environment, on a single pulse basis, as the ultimate light ion beam fusion reactor (LIFR). Consequently, these are elements in the TDF design that are critical for many of the same reasons that they are important in reactor applications. However, in almost all ways the design of the TDF should be less demanding than a reactor. The similarity and differences between the TDF and a LIFR cavity and first wall are listed in Table X-1. As noted earlier the "per pulse" quantities are similar between the two but the power generation, repetitive quantities are absent from the TDF design. This eliminates a number of constraints from the first wall such as heat removal and tritium breeding. The first wall thickness can therefore be determined simply from strength of materials considerations.

The final engineering design of the cavity and first wall will require an extensive systems analysis that investigates the combinations of parameters that are expected in this experimental facility. For this conceptual design we use the established approach of choosing a set of design parameters that are our "best estimate" for a TDF. Using these parameters we design a first wall that meets all constraints in a consistent fashion. We then explore variations of this theme to identify parameters that strongly affect the results. Such an approach is most meaningful, given the limitations of time and resources. It necessitates the quantitative investigation of synergistic effects while minimizing the very detailed design considerations of any single component.

Table X-1

Comparison of Target Development Facility and Light Ion Beam Reactor First Wall and Cavity

TDF	LIFR
• Expected lifetime is 10^3-10^4 shots	• Expected lifetime is 10^{10} shots
• Maximum stress per pulse and fatigue considerations control wall lifetime	• Maximum stress and fatigue coupled to radiation damage control wall lifetime
• No first wall cooling	• Active cooling of first wall is necessary
• No blanket behind the first wall	• Blanket behind the first wall
• No tritium breeding	• Tritium breeding is essential
• Wall thickness is determined only from strength of materials considerations	• Wall thickness is determined by strength of materials plus neutronics
• Target yield of 100-200 MJ	• Target yield of 100-200 MJ
• Wide range of cavity gas characteristics will be explored	• Narrow range of cavity gas characteristics is expected
• Cavity gas must support channel formation and ion beam propagation on a single pulse basis	• Cavity gas must support channel formation and ion beam propagation on a repetitive basis
• Cavity gas has essentially an infinite time to cool between pulses	• Cavity gas must be cooled to reasonably low temperatures in a fraction of a second or be pumped from the cavity
• First wall must be chemically compatible with cavity environment	• First wall must be chemically compatible with cavity environment
• First wall must accommodate diagnostics	• Few diagnostics will be introduced into the cavity

The constraints on the cavity and first wall design are given in Table X-2. Several choices are implicit within this set of constraints. The shot rate and operational lifetime of the facility have been chosen to be consistent with the Military Applications program plan. It is expected that this facility will cost $200 M - $500 M. It must be capable of testing several targets per day to justify this cost. We have chosen to design the first wall to survive for the lifetime of the facility. The target yield and number of ion beams are chosen to be consistent with the current understanding of target physics, driver development, and beam propagation. In this facility we choose to propagate the ions from the diode to the target over a standoff distance of several meters. This is in contrast to the PBFA facilities where a diode structure internal to the cavity will allow ballistic focussing onto the target over a distance of 10-50 cm. The 10/day rapid shot rate precludes the use of this method of beam focussing in the TDF for the target explosion would certainly damage the diode structure and require its replacement between shots. This would be prohibitively time consuming and expensive to replace. It is expected that the targets will be cryogenic to help insure high yields. The combination of cryogenic targets and a cavity gas to support the beam propagation in channels requires that the targets be injected into the chamber and that the channels be initiated by laser ionization of the gas. This places constraints on the gas type. Finally, we require that the first wall be as close to the target as possible to avoid excessively long channels. This should minimize ion energy loss in the channels. However, if there is to be bunching of the beam in the channels then there is also a minimum acceptable length.

Table X-2

Constraints on the Cavity and First Wall

Wall Lifetime	5×10^4 shots
Operational Life	5 years
Target Shot Rate	10/day or 3000/year
Target Yield	100-200 MJ
Target Type	Cryogenic
Number of Ion Beams	40
Channel Initiation Mechanism	Laser Ionization
Cavity Gas Pressure	50 Torr
Cavity Gas Temperature	300 K
First Wall Radius	Small As Possible

Detailed discussions of the cavity gas response to the target explosion, first wall mechanical response to the shock overpressure and first wall thermal response to the radiative heat flux from the gas can be found in Chapters VII, VIII, and IX, respectively. The emphasis of this chapter is the synthesis of these separate analyses into a consistent first wall design.

X.B Materials Selection and Fatigue Criteria

The first wall analysis for the TDF is centered upon the use of a ferritic steel as the structural material. To be specific, the material properties of HT-9 have been used, Table X-3. Because fatigue data is not yet available for HT-9, we have used fatigue data for a more common ferritic steel, 2-1/4 Cr - 1 Mo. This data is plotted in Fig. X-1 as it appears in the nuclear materials handbook. In addition to the basic data, we have plotted two curves that represent a reduction by a factor of 20 in cycles to failure and a reduction of a factor of 2 in total strain. The fatigue life criterion that we use is then the more conservative of these two curves. This is the accepted criterion of the ASME Boiler and Pressure Vessel Code. This data represents the response of unirradiated materials. Radiation damage effects have not yet been included in this analysis.

From Fig. X-1 we see that a total strain of 0.2% is allowed for a lifetime of 5×10^4 cycles and this is determined by the factor of two lower strain criterion rather than the reduced cycles to failure criterion. In addition to these conservative assumptions we have implicitly made two other conservative assumptions. We have chosen to use the high temperature fatigue curve even though the bulk of the wall will be operating at room temperature. Secondly, the designed lifetime of 5×10^4 shots is a factor of 3 greater than the number of full yield target shots. Two thirds of these shots will be

Table X-3

Properties of HT-9

Density	7.62 gm/cm^3
Modulus of Elasticity	1.62×10^5 MPa
Poisson's Ratio	0.295
Thermal Conductivity	0.29 W/cm-°C
Specific Heat	0.75 J/gm-°C

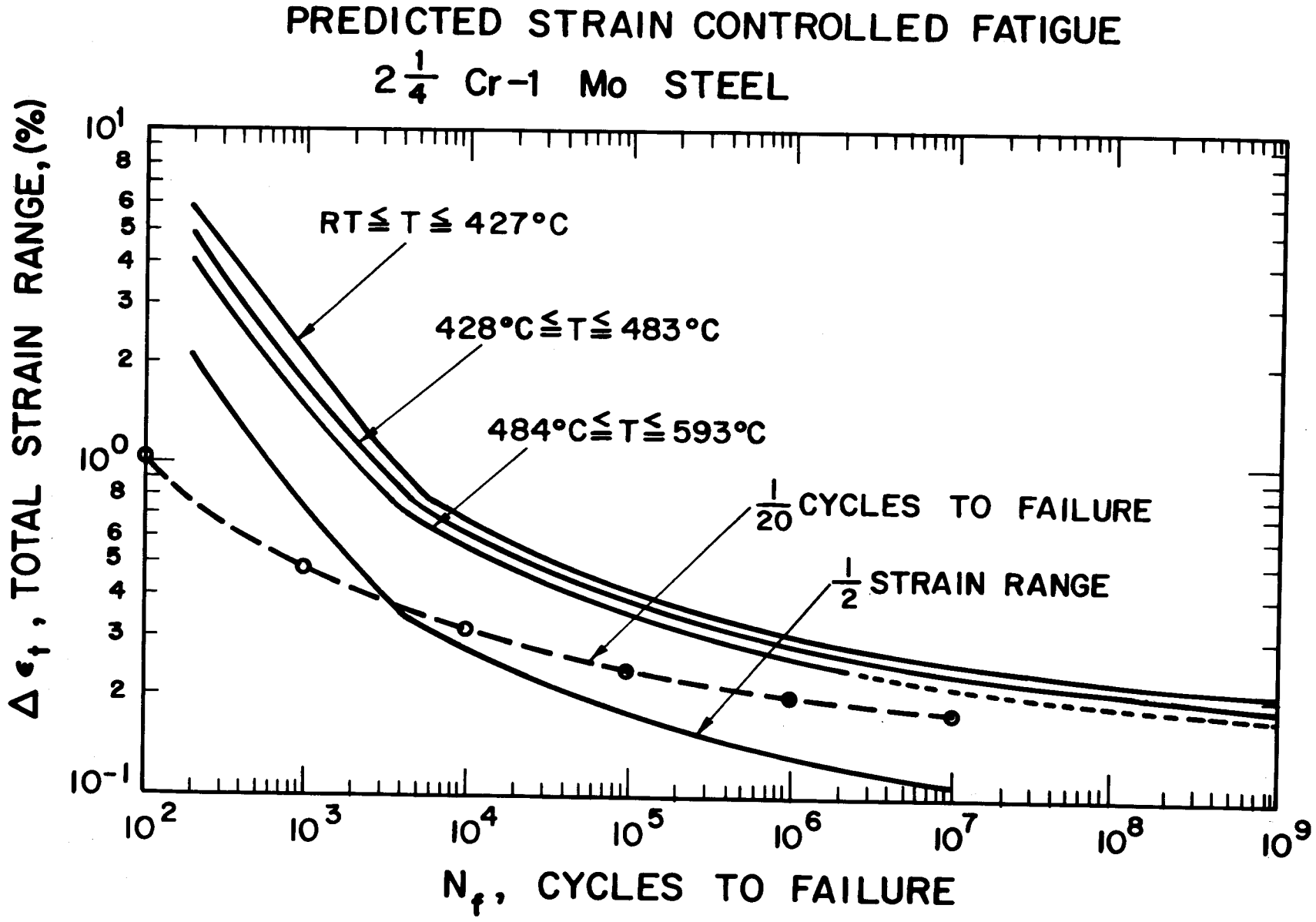
PREDICTED STRAIN CONTROLLED FATIGUE
2 1/4 Cr-1 Mo STEEL
Δεt, TOTAL STRAIN RANGE, (%)
RT ≦ T ≦ 427°C
428°C ≦ T ≦ 483°C
484°C ≦ T ≦ 593°C
1/20 CYCLES TO FAILURE
1/2 STRAIN RANGE
Nf, CYCLES TO FAILURE

Figure X-1

tests of the pulsed power driver with no high yield target in place. For these shots, the stress will be substantially less.

In fatigue studies, a cyclic uniaxial stress test is commonly used for materials characterization. Figure X-2 shows one cycle of a typical program in which σ_a and σ_m denote the alternating and mean stresses, respectively, with $\Delta\sigma$ the stress range. Normal strain (ε) is also used as the basic control parameter instead of stress. Data from such tests is the basis for the development of fatigue strength curves (i.e. the alternating stress or strain amplitude (or corresponding range) as a function of the number of cycles to failure, N_f). Portions of such curves are represented schematically in this figure to identify the effect of mean stress: a compressive mean increases the number of cycles to failure while a tensile mean has the opposite effect.

It is necessary to interpret the stress history calculated for the TDF model for comparison with specific material fatigue strength curves. The third part of Fig. X-2 is a schematic of the total stress history (thermal plus flexural) at a point such as the center of the cavity side of first wall panels. This represents, for example, three consecutive shots with the assumption that flexural stress is effectively damped out between each. It can be interpreted as response with a stress range of σ_{max} and a mean stress and alternating value both equal to $\sigma_{max}/2$. If the advantageous effect of compressive mean stress is ignored, then a fatigue life prediction should consist of a comparison of the alternating amplitude, $\sigma_{max}/2$, with the corresponding alternating stress value from the particular material fatigue curve. If the fatigue strength curve uses strain range, $\Delta\varepsilon$, and assuming essentially elastic conditions, then $\sigma_{max}/2$ should be compared with $(\Delta\varepsilon/2)E$, or simply σ_{max} with $E\Delta\varepsilon$.

Figure X-2

FATIGUE CONSIDERATIONS

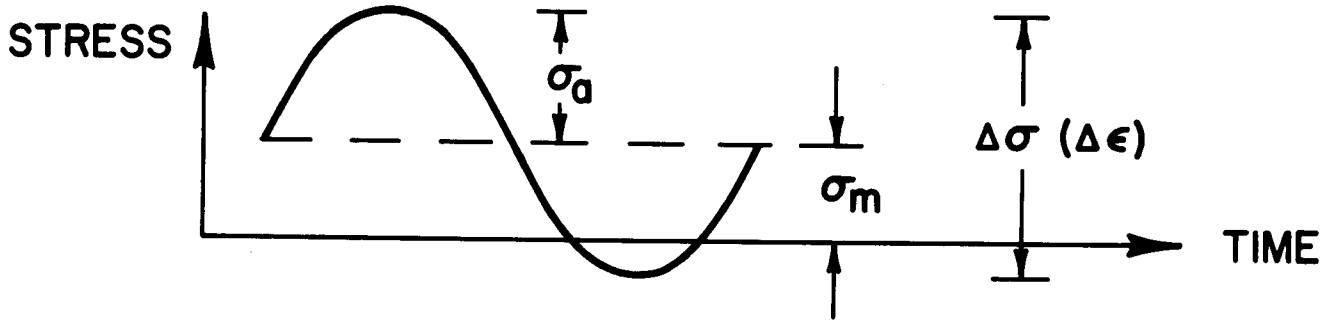

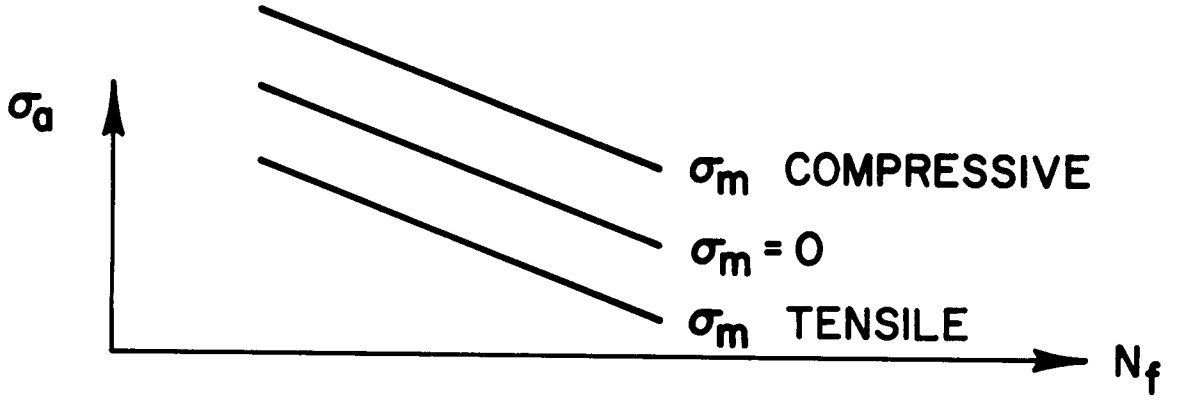

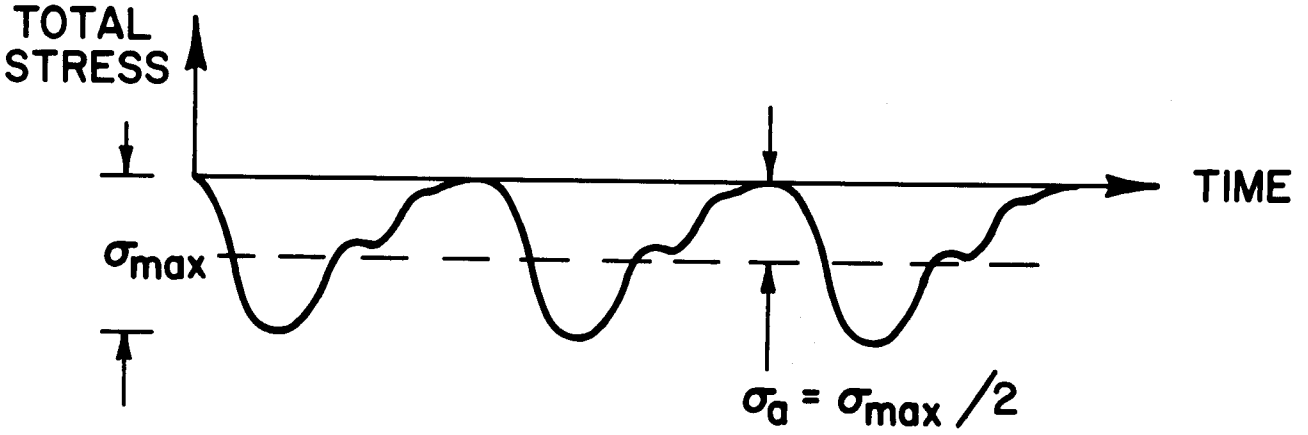

The 0.2% fatigue strain limit corresponds to a uniaxial stress of 324 MPa (48 ksi) zero to maximum. Hence, the combined effects of the thermal and mechanical stresses resulting from the incident radiative heat flux and shock overpressure must not exceed this value of 324 MPa.

In addition to the conservative use of high temperature fatigue data, a factor of three greater number of shots than expected, and the ASME boiler devaluation of the fatigue lifetime curves, it should also be noted that the lifetime curves are plotted as the logarithm of the number of shots to failure. Hence, any difference between the allowed stress levels and the actual computed stress levels will result in a much longer lifetime. This will be demonstrated later when representative values are used in this lifetime analysis.

The chemical compatibility of the first wall and the cavity environment has not yet been addressed. This will be dependent upon the pellet materials and this information is not currently available. The neutron fluence experienced by a 3 m radius wall over the lifetime of the facility is at most 9.5×10^{17} neutrons/cm^2 assuming a total of 15,000 shots at 200 MJ apiece. At this fluence level we do not expect any significant radiation damage problems that are so important in reactors when the fluence is at least 10^5 times higher.

X.C First Wall Panel and Supporting Frame Concept

The first wall in the TDF design is treated as a structure which carries the imposed dynamic pressure from the shock wave by flexural action. This is more representative of an actual design than modelling the cylindrical structure on the basis of simple thin-wall tube (membrane) theory. The wall is made up of component panels supported from behind by a rigid frame, Fig. X-3.

Figure X-3

CONCEPTUAL FIRST WALL SUPPORT STRUCTURE

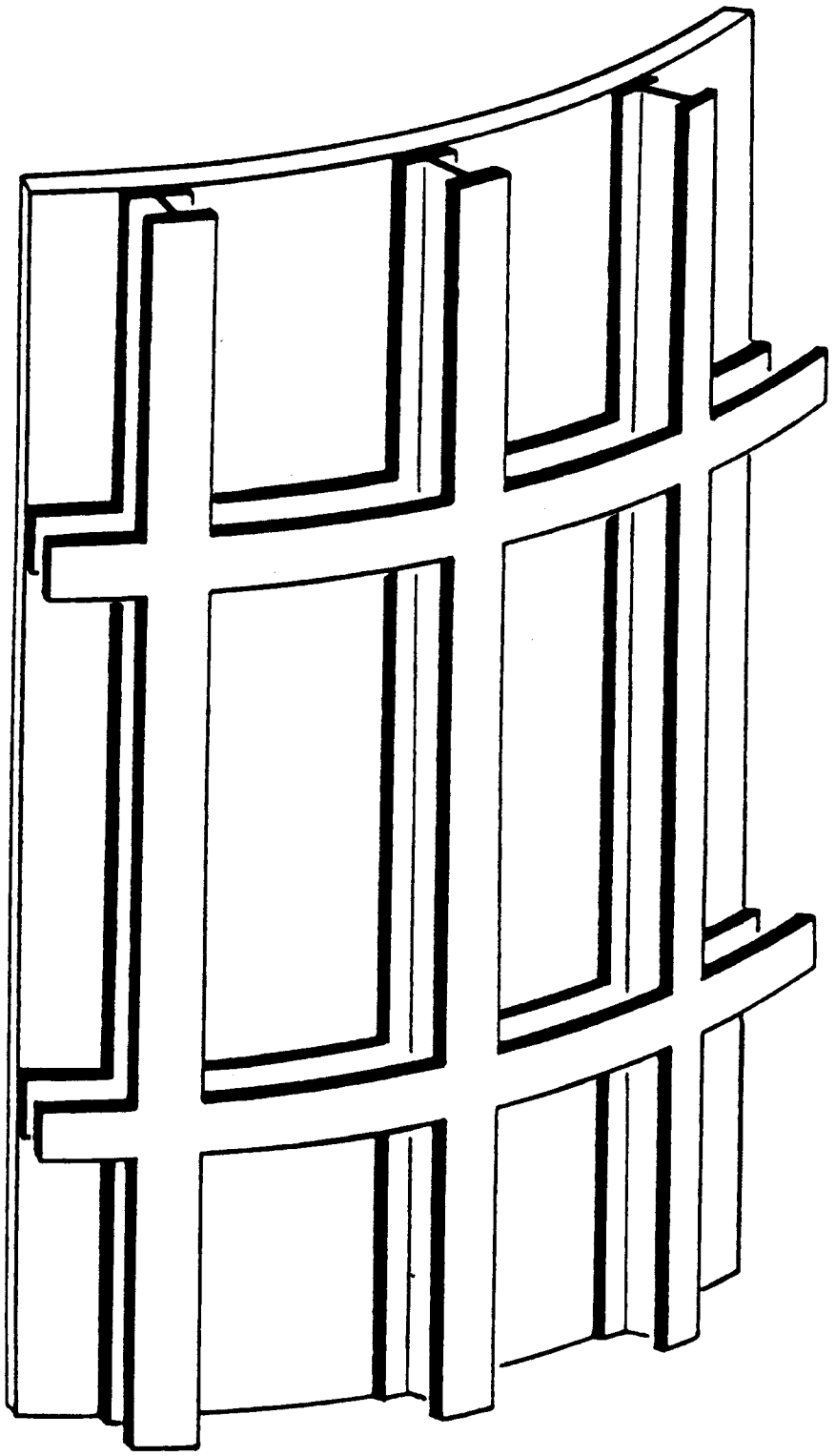

The basic design can be modified to have curved panels, cellular panels with internal cooling, scalloped panels, etc. These various design options will all fall within the scope of this analysis and are discussed in more detail in Chapter VIII.

Analysis to date has concentrated on the dynamics of the supported panel. Future work will be directed toward the structural frame. For the base design we have chosen to use a solid plate construction rather than the cellular plate. The characteristics of a specific panel design are listed in Table X-4. The panel is clamped at its vertical edges and is simply supported at its top and bottom. It is 2 m in height and has a span of 47.12 cm. Because the cavity height is 6 m, this represents a design with two circumferential ribs to support the panels between the top and bottom circumferential supports, Fig. X-3. The span is 1/40 of the circumference of the 3 m radius cavity. This allows for a single ion beam/diode structure per panel. This is somewhat arbitrarily chosen and can be easily changed. The solid panel thickness is 5 cm and the panel mass is 1 tonne. The natural frequency of this panel is 1154 Hz. The dynamic load factor accounts for the pulsed nature of the overpressure and is a function of the temporal shape of the overpressure. Its maximum value is 1.40 and thus identifies the importance of dynamic rather than simple static analysis. The pressure and heat flux experienced by the first wall at 3 m from the explosion are shown in Fig. X-4. The maximum overpressure is 11 atm (1.1 MPa) and the maximum heat flux is about 6.5 kW/cm^2 for a duration of over 0.4 ms. These result from a 200 MJ pellet yield where 60 MJ, in the form of x-rays and ions, is deposited in the gas immediately surrounding the target. The gas type in this case is 50 torr of argon mixed with 0.2 volume percent sodium. This combination of temperature rise in the wall

Table X-4

Specific First Wall Panel Parameters

Target Yield	200 MJ
Cavity Gas Pressure	50 Torr
Cavity Gas Constituents	99.8% Ar
	0.2% Na
Wall Radius	3 meters
Wall Height	6 meters
Panel Span	47.12 cm
Panel Height	6 meters
Number of Panels	40
Supported Panel Area	200 cm x 47.12 cm
Panel Thickness	5 cm
Panel Material	Ferritic Steel, HT-9
Panel Lifetime	5×10^4 shots
Allowable Stess (fatigue limit)	324 MPa
Incident Heat Flux	6.5 kW/cm^2
Incident Overpressure	1.1 MPa
Maximum Thermal Stress (Compressive)	256. MPa
Maximum Mechanical Stress at Plate Center (Compressive)	30. MPa
Maximum Total Stress at Plate Center	286. MPa
Lifetime Corresponding to Max. Stress	10^5 shots

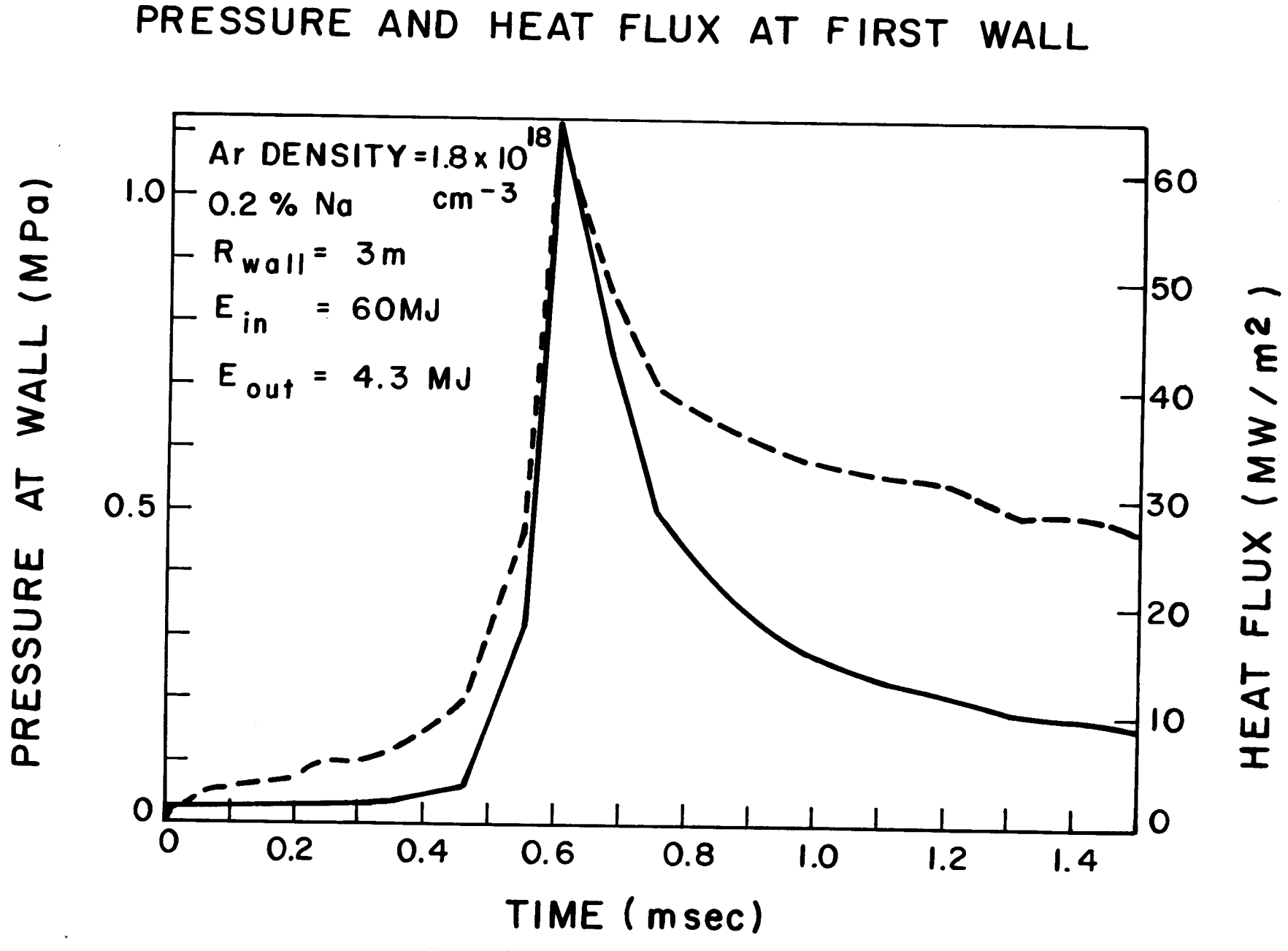
PRESSURE AND HEAT FLUX AT FIRST WALL
Ar DENSITY = 1.8 x 10^18 cm^-3
0.2 % Na
R_wall = 3m
E_in = 60MJ
E_out = 4.3 MJ
PRESSURE AT WALL (MPa)
HEAT FLUX (MW/m2)
TIME (msec)
0
0.5
1.0
0.2
0.4
0.6
0.8
1.2
1.4
10
20
30
40
50
60

Figure X-4

and mechanical overpressure leads to the stress history shown in Fig. X-5. The maximum thermal stress is 256 MPa uniformly distributed over the surface of the plate. To this we must add the stress history from the flexural action of the plate. Here, there are differences between the center of the plate and the clamped edges. Figure X-6 shows the maximum mechanical stress across the span of the panel. We see that the worst position is in the center of the plate where the thermal and mechanical compressive stresses add to produce a maximum compressive stress of 286 MPa. However, this is well below the maximum allowable stress of 324 MPa. This specific example represents a possible worst case for an argon cavity gas mixed with sodium. For greater sodium concentrations the thermal flux is not as large and hence the thermal stresses are not as large. Pure argon gas allows the radiant energy to escape from the fireball long before the shock wave reaches the wall. In this case, the maximum thermal stress is about the same as in the 2% sodium case. Thus, the 0.2% sodium case used in the example parameters is the worst situation from the maximum total stress criterion. Even with this worst case, the stress values are comfortably within the fatigue limits. The lifetime of a panel subjected to multiple loadings of 286 MPa is 10^5 shots, a factor of two greater than the design lifetime.

X-D. Conclusions

Many conservative assumptions have been built into the first wall lifetime analysis and associated design. These include:

(1) Assuming that each shot will be of the maximum predicted yield, 200 MJ, when the most likely average yield will be 100 MJ.

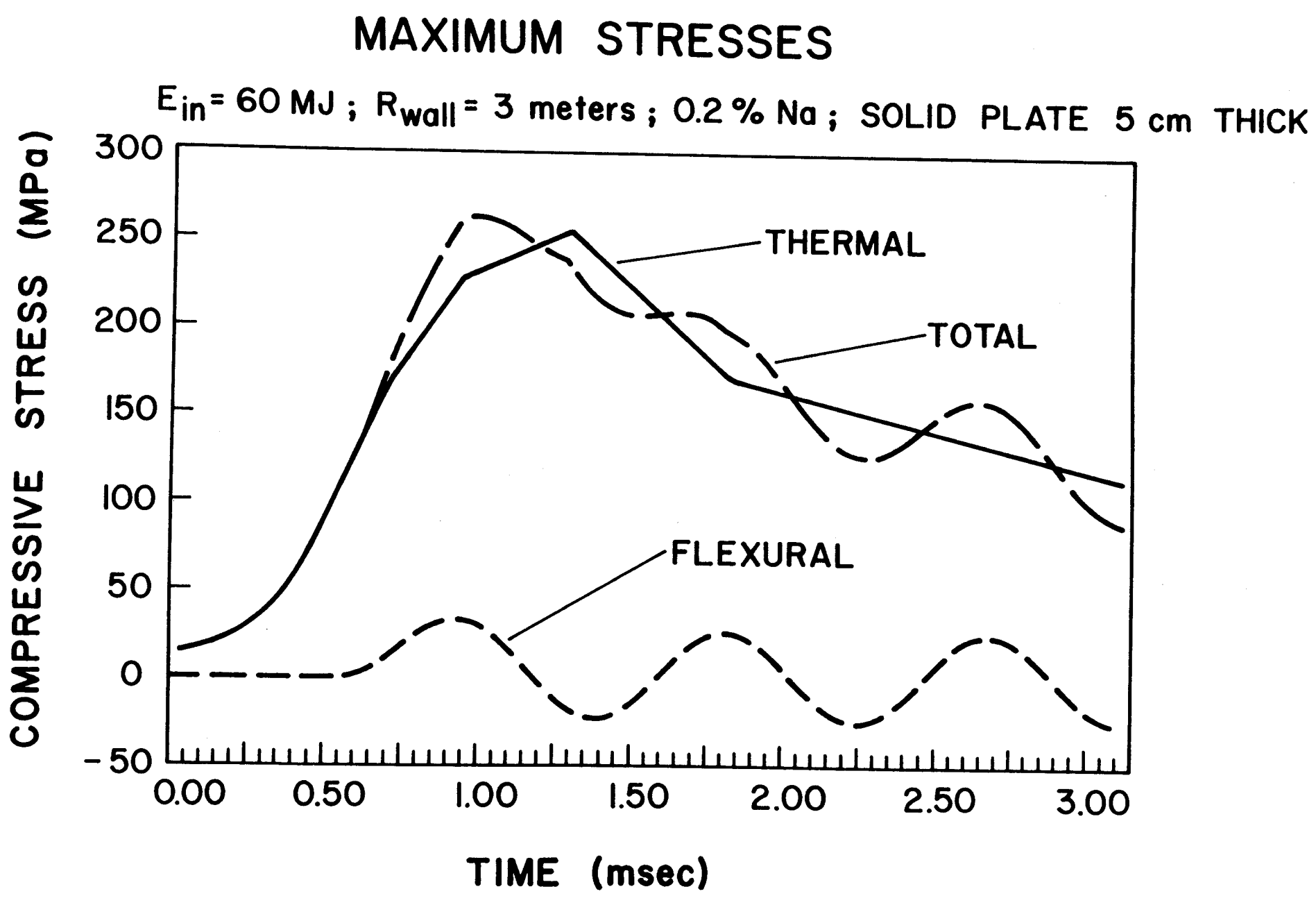
MAXIMUM STRESSES
E_{in} = 60 MJ ; R_{wall} = 3 meters ; 0.2 % Na ; SOLID PLATE 5 cm THICK
COMPRESSIVE STRESS (MPa)
300
250
200
150
100
50
0
-50
THERMAL
TOTAL
FLEXURAL
0.00
0.50
1.00
1.50
2.00
2.50
3.00
TIME (msec)

Figure X-5

Figure X-6

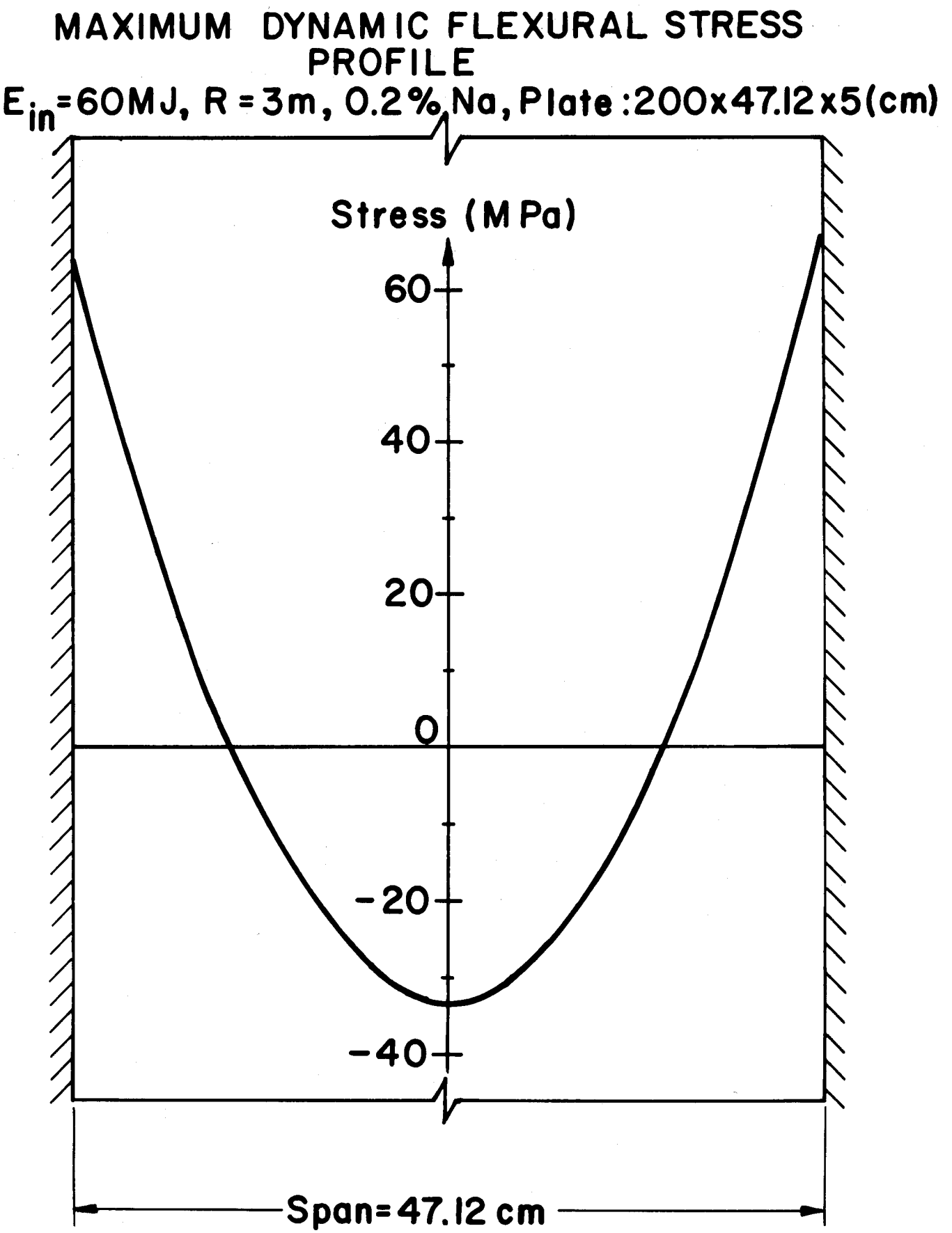
MAXIMUM DYNAMIC FLEXURAL STRESS PROFILE
E_{in}=60MJ, R=3m, 0.2% Na, Plate: 200x47.12x5(cm)
Stress (MPa)
60
40
20
0
-20
-40
Span=47.12 cm

(2) Assuming that each of the facilities 50,000 shots will result in a maximum yield explosion when only about one-third or 15,000 of these are expected to be with a target in place.

(3) Developing the fatigue lifetime data with the ASME code prescription and using the high temperature data even though the bulk of the wall will be at room temperature during the loading process.

These assumptions lead to an acceptable stress level of 324 MPa per shot. The computed stress level for a 200 MJ explosion in a 3 meter cavity filled with 50 torr of argon with 0.2 v% sodium is 286 MPa. Furthermore, parametric analysis shows that the above choice of cavity gas may be the worst possible case; hence this positive result is not jeopardized by uncertainties. The results give us confidence that the combined cavity and first wall design presented here are consistent with one another and are reasonably insensitive to uncertainties in the parameters. Stated another way, we have not identified any "show-stoppers" in the design of the cavity and first wall.

However, there are foreseeable problems that must be addressed. We note that the radiant heat flux is the greatest contributor to the stress in the first wall. This heat flux is determined to a large extent by the optical properties of the cavity gas. These are very difficult to compute accurately in the temperature and density ranges of interest and this causes concern because the heat fluxes predicted by the computer models are uncertain. On the other hand, there are straightforward design solutions to this problem including placement of a non-structural graphite liner or "curtain" on the inside surface of the first wall. This does not, therefore, rate as a "show-stopper".

The uncertainty in the blast overpressure is not as great. This is limited on the high end by strong shock theory. The computer models reproduce strong shock theory predictions when the appropriate limits are taken and we have confidence that the overpressure results (which do not correspond to a strong shock in the case of the TDF) are relatively certain.

Radiation damage effects in the first wall have not been investigated in detail. The low fluence levels experienced in the TDF would indicate that unirradiated data is appropriate. However, should the use of ferritic steel be precluded by some exotic pulsed damage effects then the design option certainly exists to change the first wall material to stainless steel for instance.

Chemical compatibility between target materials and the first wall has not been treated in any detail. This is mainly due to lack of information concerning target constituent materials.

Finally, detailed design problems such as stress concentrations, welds, etc. have not been assessed. This level of detail is beyond the scope of this report.

ACKNOWLEDGMENT

Support for this work has been provided by Sandia National Laboratory.